Table 1 (*Continued*)

Cell line	*HDAC inhibitor (μM)*	*Apoptotic cell[a] (%)*	*Cell cycle distribution[a](%)*			
			sub G_1	*G_1*	*S*	*G_2/M*
ILKM-2	Untreated control	7.35	4.07	58.61	13.05	22.89
	SAHA					
	3 μM	7.84	8.97	61.53	6.23	22.12
	30 μM	21.41	20.63	51.10	12.71	13.88
	NCH-51					
	3 μM	8.71	6.04	63.21	6.93	22.45
	30 μM	30.04	20.54	51.45	12.15	15.13

Abbreviations: HDAC, histone deacetylase; SAHA, suberoylanilide hydroxamic acid.
[a]Each value shows the average of 20 000 cells counted.

NCH-51 induces cytotoxic effect through the modulation of intracellular ROS

From the results of proteome analyses, NCH-51 appeared to promote the expression of antioxidant molecules, either at the transcriptional or post-transcriptional level, which prompted us to examine the effect of NCH-51 on the levels of ROS accumulation. Interestingly, the temporal profile of ROS amount in U266 cells treated with NCH-51 appeared to be in a concave shape indicating a gradual suppression of ROS accumulation within the initial 4 h and subsequent induction of ROS (Figure 3a), whereas the temporal profile with SAHA continuously declined over time. Similar trends were observed with other cell lines (data not shown). As summarized in Table 2, SAHA was more effective in reducing ROS than NCH-51, and the difference in ROS amount between NCH-51 and SAHA was most evident at 24 h, when the difference in growth inhibitory effect could be observed (Figure 1). These results suggested a possibility that dynamic state of ROS in each cell could be attributed to the growth inhibitory effect of HDACi. We thus examined whether NAC, a small-molecule antioxidant compound, could modulate the effect of NCH-51 (Figure 3b). Expectedly, when U266 cells were pretreated with NAC, the NCH-51-mediated cell growth inhibition was abolished. Similar effect was observed in SAHA-treated cells as much as in NCH-51-treated cells (data not shown). These results indicated that high amount of ROS might be necessary for the induction of NCH-51-mediated cytotoxicity.

Discussion

There have been accumulating reports of successful inhibition of cancer cell growth using small-molecule HDACi compounds.[1,7] Initial studies with SAHA indicated that the mode of action of HDACi might be through upregulating the transcriptionally repressed genes during carcinogenic processes by acetylating the repressive histones.[12–14] However, recent reports have demonstrated that HDACi compounds also exert anticancer effects through acetylation of non-histone substrates.[15–19] For example, HDAC6, a microtubule-associated deacetylase, was shown to be responsible for transportation of misfolded proteins to aggresome thus promoting protein degradation.[19,29] Thus, we have attempted to clarify the mechanism of anticancer effects of NCH-51 by examining both mRNA and protein levels.

In this study, we noticed that NCH-51 induced apoptosis in sensitive cell lines greater than SAHA (Figures 1 and 2a and Table 1). Analyses of mRNA expression levels in NCH-51- and SAHA-treated cells has revealed that transcriptional repression of antiapoptotic genes, such as *survivin*, *bcl-w* and *c-FLIP* and upregulation of cell cycle regulators, such as *p21* and *p19*, could be attributable to the induction of apoptosis and cell cycle arrest, respectively (Supplementary Table 1, 2 and Supplementary Figure 1), supporting the previous findings by others.[12–14] There was no difference in the mRNA expression level between NCH-51- and SAHA-treated samples (Supplementary Figure 1). We have confirmed no difference in inducing activity for acetylation of histone H4 between these two HDACi's (Supplementary Figure 2). These findings suggest that NCH-51 and SAHA similarly affect gene expression presumably through histone acetylation. We thus examined the effects of these compounds on protein expression profile to understand the difference between NCH-51 and SAHA at the post-transcriptional level.

Interestingly, our proteome analyses revealed the upregulation of some antioxidant molecules including PRDX1, PRDX2 and GSTP1-1 (Table 2 and Figure 2). In addition, previous reports indicated that some other proteins identified by the present proteome analysis (Table 2) could be activated by oxidative stress.[30–34] For example, NDPKA is reported to be activated by ROS and protected the cell from ROS-induced apoptosis.[30,31] CLIC1 protein contains a redox-active site and is activated during ROS-triggered apoptosis.[32,33] These findings suggested a possibility that NCH-51 might induce the cytotoxic effect by modulating the intracellular ROS content. In fact, pretreatment with NAC abolished the growth inhibitory effect of NCH-51 (Figure 3b). These results support the previous findings by others, which showed the ROS accumulation by HDACi.[14,34,35] However, in contrast to the previous reports, both NCH-51 and SAHA downregulated the ROS content after 24 h treatment in most of the cell lines tested except for KM5 cells, in which ROS was increased by the treatment with SAHA or NCH-51 (Table 3). These findings were reproducibly observed. Although we currently do not know the reason why there was a discrepancy between our study and others, we think the time-point and/or cell characteristics may be different between them. When temporal profiles of ROS accumulation were examined (Figure 3a), we found a typical bimodal kinetics of the intracellular ROS content after treatment with NCH-51; an initial downregulation and subsequent upregulation of ROS. On the other hand, SAHA did not follow the similar kinetics and the intracellular ROS level gradually and continuously decreased (Figure 3a). Therefore, it is possible that apparent differences in the ability of cell growth inhibition between NCH-51 and SAHA, may be explained through the different effects on the redox status of cells and induction of antioxidant proteins. Interestingly, our proteome/transcriptome analyses have revealed that the upregulation of antioxidant molecules occurred at either protein or mRNA levels: GSTP1-1 was upregulated by

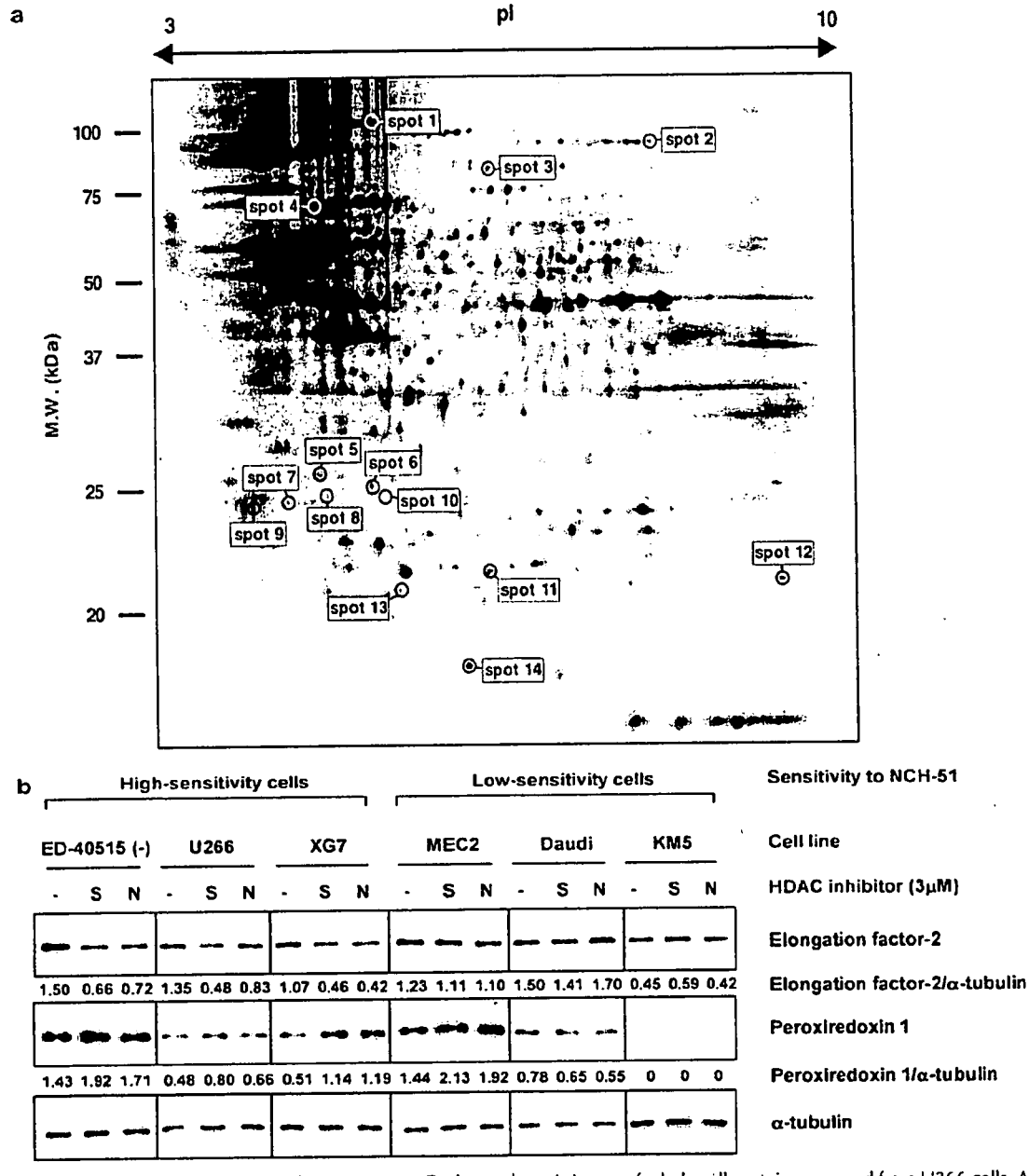

Figure 2 Proteome analysis of the effects of NCH-51. (a). 2D electrophoresis image of whole cell proteins prepared from U266 cells. After U266 cells were treated with or without 3 μM NCH-51 for 18 h, the whole cell extracts were prepared and applied to 2D electrophoresis in quadruplicates. Fourteen spots, whose relative amounts were either increased or decreased by the treatment with NCH-51 in all four gels, were indicated. Each spot number in the image corresponds to those in Table 2. MW, molecular weight (kDa). pI, isoelectric point. (b) Downregulation of elongation factor-2 (EF-2) and upregulation of peroxiredoxin 1 (PRDX1) by HDACi. The cells were treated with suberoylanilide hydroxamic acid (S) or NCH-51 (N) (3 μM) for 18 h. Whole cell extracts were prepared and subjected to immunoblots with the indicated antibodies. Each value means the ratio of the protein amount to α-tubulin (internal control).

NCH-51 only at the protein level, and PRDX1 and PRDX2 were upregulated primarily at the transcriptional level. These findings suggest that there may be two consequent antioxidative mechanisms by which HDACi modulate ROS accumulation: (i) the mRNA level, acting through induction of transcription of antioxidant molecules *de novo*, and (ii) the protein level, which was presumably caused by blocking the cellular protein transport/degradation pathway involving aggresome and proteasome. Importantly, we have observed that SAHA but not NCH-51 could induce acetylations of α-tubulin and HSP90 (Supplementary Figure 2), suggesting that SAHA might prolong the latter mechanism through blocking the degradation of antioxidant molecules. In fact, SAHA seemed to increase protein expression of PRDX1 greater than NCH-51 (Figure 2b). Since NCH-51 does not retain antioxidant molecules at the protein level, it induces the accumulation of ROS. Cellular levels of antioxidant molecules have been reported to be associated with the sensitivity to conventional anticancer agents.[36] Therefore,

Table 2 Upregulated/downregulated proteins after the treatment with NCH-51 in U266 cells

Spot no.	*Protein ID*	*Protein name*	*MW*	*pI*	*Protein ratio (T/C)*[a]	*mRNA ratio (T/C)*[a]
1	NP_001596	Alanyl-tRNA synthetase (AARS)	106734	5.31	0.80	0.74
2	NP_001952	Elongation factor-2 (EF-2)	95146	6.42	0.82	1.23
3	NP_006830	Mitochondrial inner membrane protein (IMMT)	83626	6.08	0.83	0.64
4	NP_006588	Heat-shock 70 kDa protein 8 (HSPA8)	70854	5.28	0.82	1.18
5	NP_001279	Cl^- intracellular channel protein 1 (CLIC1)	26775	5.09	1.34	0.67
6	NP_002809	Protease activator 28 β subunit (PA28β)	27213	5.44	1.54	1.03
7	NP_004300	Rho GDP-dissociation inhibitor 1 (Rho GDIα)	23193	5.02	1.42	0.92
8	NP_002779	Proteasome subunit α type3	28284	5.19	1.32	0.73
9	NP_663723	14-3-3 ζ/δ (PKC inhibitor protein 1)	28828	4.73	1.37	0.83
10	NP_039234	CI intracellular channel protein 4 (CLIC4)	28754	5.45	1.38	0.86
11	NP_000843	Glutathione *S*-transferase P 1–1(GSTP1-1)	23210	5.44	1.38	0.98
12	NP_002565	Peroxiredoxin 1 (thioredoxin peroxidase 2) (PRDX1)	22096	8.27	1.30	1.4
13	NP_005800	Peroxiredoxin 2 (thioredoxin peroxidase 1) (PRDX2)	21747	5.67	1.30	1.35
14	NP_000260	Nucleoside disphosphate kinase A (NDPKA)	17138	5.83	1.50	1.04

[a]The results are indicated as the ratio of NCH-51-treated sample to untreated control (T/C).

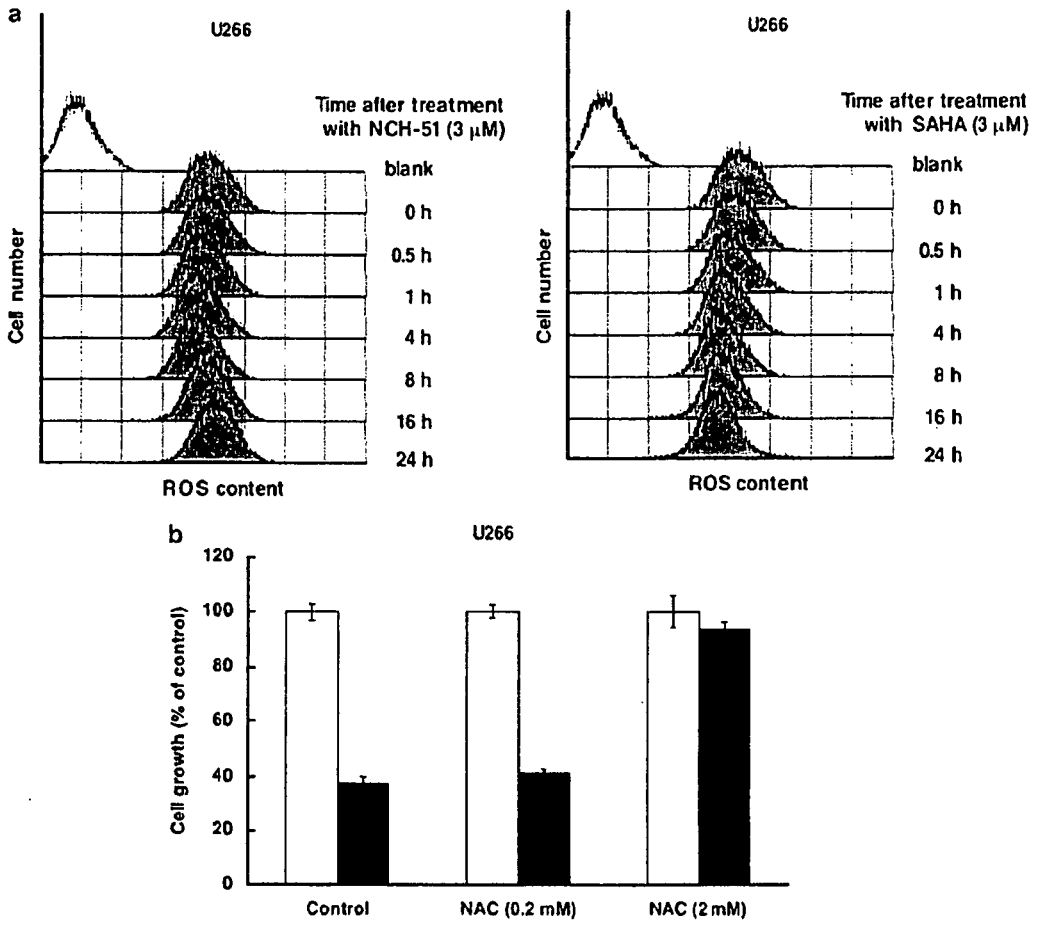

Figure 3 Effects of NCH-51 and suberoylanilide hydroxamic acid (SAHA) on reactive oxygen species (ROS) accumulation. (a) Time course of intracellular ROS after the treatment with HDACi. U266 cells were treated with NCH-51 or SAHA (3 μM) given the indicated time (0–24 h). After the treatment, H_2-DCFDA was added and further incubated for 30 min. ROS content was measured by flowcytometry. Blank, H_2-DCFDA-untreated control. (b) Effects of *N*-acetyl-L-cysteine (NAC) on the NCH-51-induced cell growth inhibition. U266 cells were treated with or without NCH-51 (3 μM) for 24 h in the presence or absence of NAC (0.2 or 2 mM). Cell growth was measured by 3-(4,5-dimethylthiazol-2-yl)-2,5-diphenyltetrazolium bromide assay. Open and closed bars indicate untreated and the NCH-51-treated cells. The results are shown as the percentage compared to untreated control. Experiments were done in triplicates and the mean values $\pm$ s.d. are shown.

NCH-51 can not only induce apoptosis through ROS accumulation, but also enhance the cytotoxicity of other agents in the combination treatment more efficiently than SAHA.

Our proteome analysis has also identified several proteins other than antioxidant molecules, including EF-2, AARS and HSPA8. We confirmed that EF-2 protein, a member of the GTP-

Table 3 ROS content and growth inhibitory effect after the treatment with HDAC inhibitor

Cell line	ROS content (% of control)[a]		Growth inhibition (% of control)[b]	
	NCH-51 (3 μM)	SAHA (3 μM)	NCH-51 (3 μM)	SAHA (3 μM)
Jurkat	86	47	63.5±0.8	37.7±2.5
MT-2	100	100	38.8±0.3	11.0±2.3
ED-40515 (−)	82	56	71.2±1.2	44.1±1.0
MEC2	59	46	41.3±1.1	3.5±2.8
MO1043	91	65	46.0±0.5	7.2±2.9
Daudi	74	54	25.6±1.8	15.1±3.0
U266	95	85	80.7±1.8	51.7±3.2
XG7	74	28	66.5±1.1	23.1±1.6
KM5	126	119	20.5±0.5	14.6±1.2
ILKM-2	94	94	85.5±0.2	81.3±1.1

Abbreviations: HDAC, histone deacetylase; ROS, reactive oxygen species; SAHA, suberoylanilide hydroxamic acid.
[a]Each value shows the average of 20 000 cells counted.
[b]Each value shows the mean±s.d.

binding translational elongation factor family,[37] was specifically decreased in high-sensitivity cell lines such as ED-40515 (−) and U266 cells (Figure 2b) after 16 h treatment (data not shown). However, gene expression of EF-2 was upregulated after the treatment with NCH-51 (Table 2). This discrepancy indicates a possibility that NCH-51 could induce rapid turnover of EF-2 protein followed by upregulation of RNA expression. Similar effects on EF-2 were also observed with SAHA (Figure 2b). Since EF-2 has been reported to be inactivated by ROS and lead to inhibition of translation,[38] it is suggested that locally induced ROS by HDACi might induce EF-2 inactivation and degradation presumably by direct oxidation. Although the mechanism by which EF-2 is downregulated by HDACi remains unclear, EF-2 may be used as a feasible surrogate marker to evaluate the susceptibility of HDACi. Similar to EF-2, AARS and HSPA8 were downregulated at the protein level. It is known that HSPA8 are involved in protein folding and transport.[39] Thus, these findings collectively suggest that NCH-51 might arrest protein synthesis and transportation.

In conclusion, our study demonstrates the therapeutic advantage of NCH-51 on growth inhibition of lymphoid malignant cells. Importantly, NCH-51 did not affect the cell growth of normal PBMCs with the effective concentrations on malignant cells (Figure 1b). In addition to its therapeutic efficacy and selectivity, NCH-51 has additional advantages in clinical use based on its pharmacological features. Therefore, NCH-51 could be a useful anticancer agent against lymphoid malignancies.

Acknowledgements

We thank Mr ME Cueno for language editing. This work is supported in part by grant-in-aids from the Ministry of Education, Culture, Sports, Science and Technology and the Ministry of Health, Labor and Welfare of Japan. TS is supported by a grant of Aichi Cancer Research Foundation and a grant of Oujinkai Foundation. HN, TS and NY are supported by a grant of Takeda Science Foundation.

References

1 Minucci S, Pelicci PG. Histone deacetylase inhibitors and the promise of epigenetic (and more) treatments for cancer. *Nat Rev Cancer* 2006; **6**: 38–51.
2 Strahl BD, Allis CD. The language of covalent histone modifications. *Nature* 2000; **403**: 41–45.
3 Turner BM. Cellular memory and the histone code. *Cell* 2002; **111**: 285–291.
4 Claus R, Lubbert M. Epigenetic targets in hematopoietic malignancies. *Oncogene* 2003; **22**: 6489–6496.
5 Fraga MF, Ballestar E, Villar-Garea A, Boix-Chornet M, Espada J, Schotta G *et al*. Loss of acetylation at Lys16 and trimethylation at Lys20 of histone H4 is a common hallmark of human cancer. *Nat Genet* 2005; **37**: 391–400.
6 Seligson DB, Horvath S, Shi T, Yu H, Tze S, Grunstein M *et al*. Global histone modification patterns predict risk of prostate cancer recurrence. *Nature* 2005; **435**: 1262–1266.
7 Kelly WK, Marks PA. Drug insight: histone deacetylase inhibitors–development of the new targeted anticancer agent suberoylanilide hydroxamic acid. *Nat Clin Pract Oncol* 2005; **2**: 150–157.
8 Kelly WK, O'Connor OA, Krug LM, Chiao JH, Heaney M, Curley T *et al*. Phase I study of an oral histone deacetylase inhibitor, suberoylanilide hydroxamic acid, in patients with advanced cancer. *J Clin Oncol* 2005; **23**: 3923–3931.
9 Ryan QC, Headlee D, Acharya M, Sparreboom A, Trepel JB, Ye J *et al*. Phase I and pharmacokinetic study of MS-275, a histone deacetylase inhibitor, in patients with advanced and refractory solid tumors or lymphoma. *J Clin Oncol* 2005; **23**: 3912–3922.
10 Golub LM, Lee HM, Ryan ME, Giannobile WV, Payne J, Sorsa T. Tetracyclines inhibit connective tissue breakdown by multiple non-antimicrobial mechanisms. *Adv Dent Res* 1998; **12**: 12–26.
11 Suzuki T, Nagano Y, Kouketsu A, Matsuura A, Maruyama S, Kurotaki M *et al*. Novel inhibitors of human histone deacetylases: design, synthesis, enzyme inhibition, and cancer cell growth inhibition of SAHA-based non-hydroxamates. *J Med Chem* 2005; **48**: 1019–1032.
12 Huang L, Sowa Y, Sakai T, Pardee AB. Activation of the p21WAF1/CIP1 promoter independent of p53 by the histone deacetylase inhibitor suberoylanilide hydroxamic acid (SAHA) through the Sp1 sites. *Oncogene* 2000; **19**: 5712–5719.
13 Richon VM, Sandhoff TW, Rifkind RA, Marks PA. Histone deacetylase inhibitor selectively induces p21WAF1 expression and gene-associated histone acetylation. *Proc Natl Acad Sci USA* 2000; **97**: 10014–10019.
14 Rosato RR, Almenara JA, Grant S. The histone deacetylase inhibitor MS-275 promotes differentiation or apoptosis in human leukemia cells through a process regulated by generation of reactive oxygen species and induction of p21CIP1/WAF1 1. *Cancer Res* 2003; **63**: 3637–3645.
15 Bali P, Pranpat M, Bradner J, Balasis M, Fiskus W, Guo F *et al*. Inhibition of histone deacetylase 6 acetylates and disrupts the chaperone function of heat shock protein 90: a novel basis for antileukemia activity of histone deacetylase inhibitors. *J Biol Chem* 2005; **280**: 26729–26734.
16 Hubbert C, Guardiola A, Shao R, Kawaguchi Y, Ito A, Nixon A *et al*. HDAC6 is a microtubule-associated deacetylase. *Nature* 2002; **417**: 455–458.

17 Insinga A, Monestiroli S, Ronzoni S, Carbone R, Pearson M, Pruneri G *et al.* Impairment of p53 acetylation, stability and function by an oncogenic transcription factor. *EMBO J* 2004; **23**: 1144–1154.
18 Chen L, Fischle W, Verdin E, Greene WC. Duration of nuclear NF-kappaB action regulated by reversible acetylation. *Science* 2001; **293**: 1653–1657.
19 Hideshima T, Bradner JE, Wong J, Chauhan D, Richardson P, Schreiber SL *et al.* Small-molecule inhibition of proteasome and aggresome function induces synergistic antitumor activity in multiple myeloma. *Proc Natl Acad Sci USA* 2005; **102**: 8567–8572.
20 Sanda T, Asamitsu K, Ogura H, Iida S, Utsunomiya A, Ueda R *et al.* Induction of cell death in adult T-cell leukemia cells by a novel IkappaB kinase inhibitor. *Leukemia* 2006; **20**: 590–598.
21 Uranishi M, Iida S, Sanda T, Ishida T, Tajima E, Ito M *et al.* Multiple myeloma oncogene 1 (MUM1)/interferon regulatory factor 4 (IRF4) upregulates monokine induced by interferon-gamma (MIG) gene expression in B-cell malignancy. *Leukemia* 2005; **19**: 1471–1478.
22 Pulvertaft JV. Cytology of Burkitt's tumour (African lymphoma). *Lancet* 1964; **39**: 238–240.
23 Klein E, Klein G, Nadkarni JS, Nadkarni JJ, Wigzell H, Clifford P. Surface IgM-kappa specificity on a Burkitt lymphoma cell *in vivo* and in derived culture lines. *Cancer Res* 1968; **28**: 1300–1310.
24 Suzuki A, Iida S, Kato-Uranishi M, Tajima E, Zhan F, Hanamura I *et al.* ARK5 is transcriptionally regulated by the Large-MAF family and mediates IGF-1-induced cell invasion in multiple myeloma: ARK5 as a new molecular determinant of malignant multiple myeloma. *Oncogene* 2005; **24**: 6936–6944.
25 Sanda T, Iida S, Ogura H, Asamitsu K, Murata T, Bacon KB *et al.* Growth inhibition of multiple myeloma cells by a novel IkappaB kinase inhibitor. *Clin Cancer Res* 2005; **11**: 1974–1982.
26 Seike M, Kondo T, Mori Y, Gemma A, Kudoh S, Sakamoto M *et al.* Proteomic analysis of intestinal epithelial cells expressing stabilized beta-catenin. *Cancer Res* 2003; **63**: 4641–4647.
27 Imai K, Nakata K, Kawai K, Hamano T, Mei N, Kasai H *et al.* Induction of OGG1 gene expression by HIV-1 Tat. *J Biol Chem* 2005; **280**: 26701–26713.
28 Opferman JT, Korsmeyer SJ. Apoptosis in the development and maintenance of the immune system. *Nat Immunol* 2003; **4**: 410–415.
29 Kawaguchi Y, Kovacs JJ, McLaurin A, Vance JM, Ito A, Yao TP. The deacetylase HDAC6 regulates aggresome formation and cell viability in response to misfolded protein stress. *Cell* 2003; **115**: 727–738.
30 Song EJ, Kim YS, Chung JY, Kim E, Chae SK, Lee KJ. Oxidative modification of nucleoside diphosphate kinase and its identification by matrix-assisted laser desorption/ionization time-of-flight mass spectrometry. *Biochemistry* 2000; **39**: 10090–10097.
31 Arnaud-Dabernat S, Masse K, Smani M, Peuchant E, Landry M, Bourbon PM *et al.* Nm23-M2/NDP kinase B induces endogenous c-myc and nm23-M1/NDP kinase A overexpression in BAF3 cells. Both NDP kinases protect the cells from oxidative stress-induced death. *Exp Cell Res* 2004; **301**: 293–304.
32 Harrop SJ, DeMaere MZ, Fairlie WD, Reztsova T, Valenzuela SM, Mazzanti M *et al.* Crystal structure of a soluble form of the intracellular chloride ion channel CLIC1 (NCC27) at 1.4-A resolution. *J Biol Chem* 2001; **276**: 44993–45000.
33 Shimizu T, Numata T, Okada Y. A role of reactive oxygen species in apoptotic activation of volume-sensitive Cl(−) channel. *Proc Natl Acad Sci USA* 2004; **101**: 6770–6773.
34 Ruefli AA, Ausserlechner MJ, Bernhard D, Sutton VR, Tainton KM, Kofler R *et al.* The histone deacetylase inhibitor and chemotherapeutic agent suberoylanilide hydroxamic acid (SAHA) induces a cell-death pathway characterized by cleavage of Bid and production of reactive oxygen species. *Proc Natl Acad Sci USA* 2001; **98**: 10833–10838.
35 Ungerstedt JS, Sowa Y, Xu WS, Shao Y, Dokmanovic M, Perez G *et al.* Role of thioredoxin in the response of normal and transformed cells to histone deacetylase inhibitors. *Proc Natl Acad Sci USA* 2005; **102**: 673–678.
36 Yokomizo A, Ono M, Nanri H, Makino Y, Ohga T, Wada M *et al.* Cellular levels of thioredoxin associated with drug sensitivity to cisplatin, mitomycin C, doxorubicin, and etoposide. *Cancer Res* 1995; **55**: 4293–4296.
37 Ryazanov AG, Shestakova EA, Natapov PG. Phosphorylation of elongation factor 2 by EF-2 kinase affects rate of translation. *Nature* 1988; **334**: 170–173.
38 Patel J, McLeod LE, Vries RG, Flynn A, Wang X, Proud CG. Cellular stresses profoundly inhibit protein synthesis and modulate the states of phosphorylation of multiple translation factors. *Eur J Biochem* 2002; **269**: 3076–3085.
39 Young JC, Agashe VR, Siegers K, Hartl FU. Pathways of chaperone-mediated protein folding in the cytosol. *Nat Rev Mol Cell Biol* 2004; **5**: 781–791.

Supplementary Information accompanies the paper on the Leukemia website (http://www.nature.com/leu)

Available online at www.sciencedirect.com
ScienceDirect
ELSEVIER
Mutation Research 619 (2007) 113–123
MR
Fundamental and Molecular Mechanisms of Mutagenesis
www.elsevier.com/locate/molmut
Community address: www.elsevier.com/locate/mutres

Potassium bromate treatment predominantly causes large deletions, but not GC > TA transversion in human cells

Yang Luan [a,b,c], Takayoshi Suzuki [a], Rajaguru Palanisamy [a,d], Yoshio Takashima [b], Hiroko Sakamoto [b], Mayumi Sakuraba [b], Tomoko Koizumi [b], Mika Saito [b,e], Hiroshi Matsufuji [e], Kazuo Yamagata [e], Teruhide Yamaguchi [a], Makoto Hayashi [b], Masamitsu Honma [b,*]

[a] *Division of Cellular and Gene Therapy Products, National Institute of Health Sciences, 1-18-1 Kamiyoga, Setagaya-ku, Tokyo 158-8501, Japan*
[b] *Division of Genetics and Mutagenesis, National Institute of Health Sciences, 1-18-1 Kamiyoga, Setagaya-ku, Tokyo 158-8501, Japan*
[c] *Center for Drug Safety Evaluation, Shanghai Institute of Materia Medica, Chinese Academy of Sciences, 294 Tai-Yuan Road, Shanghai 200031, China*
[d] *Department of Biotechnology, School of Engineering and Technology, Bharathidasan University, Palkalaiperur, Tiruchirappalli 620024, India*
[e] *Department of Food Science and Technology, College of Bioresource Sciences, Nihon University, 1866 Kameino, Fujisawa-shi, Kanagawa 252-8510, Japan*

Received 21 October 2006; received in revised form 24 February 2007; accepted 28 February 2007
Available online 4 March 2007

Abstract

Potassium bromate ($KBrO_3$) is strongly carcinogenic in rodents and mutagenic in bacteria and mammalian cells in vitro. The proposed genotoxic mechanism for $KBrO_3$ is oxidative DNA damage. $KBrO_3$ can generate high yields of 8-hydroxydeoxyguanosine (8OHdG) DNA adducts, which cause GC > TA transversions in cell-free systems. In this study, we investigated the in vitro genotoxicity of $KBrO_3$ in human lymphoblastoid TK6 cells using the comet (COM) assay, the micronucleus (MN) test, and the thymidine kinase (*TK*) gene mutation assay. After a 4 h treatment, the alkaline and neutral COM assay demonstrated that $KBrO_3$ directly yielded DNA damages including DNA double strand breaks (DSBs). $KBrO_3$ also induced MN and *TK* mutations concentration-dependently. At the highest concentration (5 mM), $KBrO_3$ induced MN and *TK* mutation frequencies that were over 30 times the background level. Molecular analysis revealed that 90% of the induced mutations were large deletions that involved loss of heterozygosity (LOH) at the *TK* locus. Ionizing-irradiation exhibited similar mutational spectrum in our system. These results indicate that the major genotoxicity of $KBrO_3$ may be due to DSBs that lead to large deletions rather than to 8OHdG adducts that lead to GC > TA transversions, as is commonly believed. To better understand the genotoxic mechanism of $KBrO_3$, we analyzed gene expression profiles of TK6 cells using Affymetrix Genechip. Some genes involved in stress, apoptosis, and DNA repair were up-regulated by the treatment of $KBrO_3$. However, we could not observe the similarity of gene expression profile in the treatment of $KBrO_3$ to ionizing-irradiation as well as oxidative damage inducers.

Keywords: Potassium bromate ($KBrO_3$); *TK*-mutation; Loss of heterozygosity (LOH); 8-Hydroxydeoxyguanosine (8OHdG); Gene expression profile

* Corresponding author. Tel.: +81 3 3700 1141x435; fax: +81 3 3700 2348.
E-mail address: honma@nihs.go.jp (M. Honma).

0027-5107/$ – see front matter © 2007 Elsevier B.V. All rights reserved.
doi:10.1016/j.mrfmmm.2007.02.029

1. Introduction

Potassium bromate ($KBrO_3$) is used as in bread making a flour improver and in the production of fish-pastes. The EU countries now prohibit its use as a food additive because of its carcinogenicity. Japan and the USA, however, permit its use in bread making on the condition that it never remains in the final product. $KBrO_3$ causes tumors, especially in kidney, in rats, and mice after long-term oral administration in drinking water [1–3]. $KBrO_3$ is also genotoxic. It is positive in in vitro genotoxicity tests – including the bacterial reverse mutation assay [1], the chromosomal aberration test conducted in Chinese hamster cells [4], and the mouse lymphoma assay [5] – and in vivo in the micronucleus test (MN) [6,7].

It has been proposed that $KBrO_3$ induces tumors through the production of oxidative damage to DNA. Oxidative DNA damage can cause mutations that contribute to the activation of oncogenes and/or the inactivation of tumor suppressor genes, thereby leading to tumorigenesis [8,9]. 8-Hydroxydeoxyguanosine (8OHdG) is the main form of oxidative DNA damage induced by $KBrO_3$ [10]. It primarily causes GC > TA transversions (as a result of the pairing of 8OHdG with A) and is believed to be responsible for mutagenesis, carcinogenesis, and aging [11,12]. $KBrO_3$ increases 8OHdG DNA adducts in vivo and in vitro [13–15]. However, $KBrO_3$ induces mutations weakly in microbial mutation assays and the *Hprt* mutation assay in mammalian cells, while it induces chromosome aberrations strongly both in vivo and in vitro [1,16,17]. These findings raise the question of whether 8OHdG is required for the mutagenic process involved in $KBrO_3$-induced carcinogenesis.

In the present study, we examined the genotoxic properties of $KBrO_3$ using the comet assay (COM), the MN test, and thymidine kinase (*TK*) gene mutation assays in human lymphoblastoid TK6 cells [18]. Unlike the X-linked hemizygous *HPRT* gene mutation assay, the *TK* mutation assay can detect not only point mutations, but also large scale chromosomal deletions, recombinations, and aneuploidy [19–21]. Most of the genetic changes observed in *TK* mutants occur in human tumors and are presumed relevant to carcinogenesis. We analyzed the *TK* mutants induced by $KBrO_3$ at the molecular level and investigated what kind of mutation predominated. We also profiled global gene expression in TK6 cell exposed to $KBrO_3$ using Affymetrix GeneChip® Expression analysis to understand the genotoxic mechanism of $KBrO_3$.

2. Materials and methods

2.1. Cell culture, chemicals, and treatment

The TK6 human lymphoblastoid cell line has been described previously [22]. Cells were maintained in RPMI 1640 medium (Gibco-BRL, Life Technology Inc., Grand Island, NY) supplemented with 10% heat-inactivated horse serum (JR Biosciences, Lenexa, KS), 200 μg/ml sodium pyruvate, 100 U/ml penicillin, and 100 μg/ml streptomycin. The cultures were incubated at 37 °C in a 5% CO_2 atmosphere with 100% humidity. $KBrO_3$ (CAS No.7758-01-2) was purchased from Wako Pure Chemical Co. (Tokyo) and dissolved in RPMI medium just before use.

We prepared 20 ml aliquots of cell suspension at a concentration of 5.0×10^5 cells/ml in 50 ml polystyrene tubes. Different concentrations of $KBrO_3$ were added to the tubes, which were then placed on a platform shaker and incubated at 37 °C for 4 h with gentle shaking. At the end of the treatment period, the cell cultures were centrifuged, washed once, and re-suspended in fresh medium. We cultured them in new flasks for the MN assay and *TK* gene mutation assay, or diluted them for plating for survival estimates.

2.2. Genotoxicity assays

After treating cells with $KBrO_3$, we prepared slides for conducting the alkaline and neutral COM assay. The alkaline COM assay was performed as previously reported [23]. For the neutral COM assay, the slide was electrophoresed with chilled neutral solution (pH 8) containing of 90 mM Tris, 2 mM Na_2EDTA, and 90 mM boric acid according to the method by Wada et al. [24]. The COM slides were stained with SYBER green (Molecular Probes, Eugene, OR) and observed by an Olympus model BX50 fluorescence microscope. At least 50 cells were captured by CCD camera, and tail length of the comet was measured. The relationship between $KBrO_3$ treatment and migration was statistically analyzed by the Dunnett test [25].

We prepared the MN test samples 48 h after treatment, as previously reported [23]. Briefly, approximately 10^6 cells suspended in hypotonic KCl solution were incubated for 10 min at room temperature, fixed twice with ice-cold methanol containing 25% acetic acid, then re-suspended in methanol containing 1% acetic acid. A drop of the suspension was placed on a clean glass slide and air-dried. The cells were stained with 40 μg/ml acridine orange solution and immediately observed with the aid of an Olympus model BX50 fluorescence microscope equipped with a U-MWBV band pass filter. At least 1000 intact interphase cells for each treatment were examined, and the cells containing MN were scored. The MN frequencies between non-treated and treated cells were statistically analyzed by Fisher's exact test [26].

We prepared the *TK* gene mutation assay samples 3 days after treatment. We seeded cells from each culture into 96-well plates at 40,000 cells/well in the presence of 3.0 μg/ml trifluo-

rothymidine (TFT). We also plated 1.6 cells/well without TFT to determine plating efficiency. All plates were incubated at 37 °C in a humidified atmosphere of 5% CO_2 in air. After 14 days, we scored colonies on the PE plates and the normal-growing (NG) *TK* mutants on the TFT plates, then re-fed the plates containing TFT with fresh TFT, incubated them for an additional 14 days, and scored them for slow-growing (SG) *TK* mutants. Mutation frequencies, relative survival (RS), and relative suspension growth (RSG) were calculated as previously described [23]. The data of mutant frequencies were statistically analyzed by Omori's method, which consists of a modified Dunnett's procedure for identifying clear negative, a Simpson–Margolin procedure for detecting downturn data, and a trend test to evaluate the dose-dependency [27].

2.3. LOH analysis of TK mutations by polymerase chain reaction (PCR)

To avoid analyzing identical mutants, we performed an additional *TK* mutation assay and isolated *TK* mutants from independent culture after a 4 h treatment with 2.5 mM $KBrO_3$. We confirmed the phenotype of the *TK* mutant clones by re-challenging them with TFT medium. We also determined the growth rate of the clones and confirmed whether they were NG or SG mutants.

Genomic DNA was extracted from the *TK* mutant cells and used as a template for PCR. We conducted the PCR-based LOH analysis of the human *TK* gene as described previously [28]. A set of primers was used to each amplify the parts of exons 4 and 7 of the *TK* gene that is heterozygous for frame shift mutations. A third primer set for amplifying parts of the β-globin was also used as the internal control. We applied quantitative-multiple PCR for co-amplification of the three regions. The PCR products were analyzed with an ABI310 genetic analyzer (PE Biosystems, Chiba, Japan), and were classified into "no LOH", "hemizygous (hemi-) LOH", or "homozygous (homo-) LOH". To determine the extent of the LOH, we analyzed 10 microsatellite loci on chromosome 17q by PCR-based LOH analysis [28]. The results were processed by GenoTyper™ software (PE Biosystems, Chiba, Japan) according to the manufacturer's guidelines.

2.4. Gene expression analysis

Total RNA was isolated from the TK6 cells after 4 h treatment with 2.5 mM $KBrO_3$ and was purified by RNeasy columns (Qiagen, Valencia, CA). We conducted a single cDNA synthesis, cRNA labeling, and cRNA fragmentation according to the manufacturer's recommendations (Affymetrix Inc., Santa Clara, CA) and employed Affymetrix GeneChip Expression analysis. The hybridization mixture for each sample was hybridized to an Affymetrix U133A human genome array. We processed the scanned data using Microarray Suite Software Version 5.0 (Affymetrix Inc., Santa Clara, CA) and imported the data into GeneSpring software (Silicon Genetics, Redwood City, CA). Signal intensity was normalized by per-gene and per-chip, and the ratios were calculated by normalizing $KBrO_3$ sample to the corresponding control sample. We used intensity-dependent (step-wise) selection of significant changes with higher cut-off value for lower signal intensity (1.75-, 2.0-, 2.25-, 2.5-, and 3.5-fold for genes intensity range of >1000, 500–1000, 100–500, 50–100, and 10–50, respectively), and up-regulated genes with a presence call in $KBrO_3$ sample, whereas down-regulated genes with a presence call in the control sample.

3. Results

3.1. Cytotoxicity and genotoxicity of $KBrO_3$

$KBrO_3$ exerted strong and concentration-dependent cytotoxicity in TK6 cells (Fig. 1). It induced approximately 50% cytotoxicity (51% RSG and 44% RS) at 2.5 mM. To investigate whether $KBrO_3$ directly causes DNA damage, we conducted the COM assay. Induction of COM tail after the treatment of in alkaline version was statistically significant 2.5 and 5 mM. In the neutral COM assay, the induction was observed form the lower concentration (Fig. 1). Because the neutral COM is thought to be associated with DNA double strand breaks (DSBs) [29], this result indicates that $KBrO_3$ directly causes DNA damage including DSBs. $KBrO_3$ also induced MN and *TK* mutation in a concentration-dependent manner and their inductions were statistically significant (Fig. 1). At the maximum concentration, it induced both MN and *TK* mutation frequencies about 30 times the control values. Two distinct phenotypic classes of *TK* mutants were generated: NG mutants grew at the same rate as the wild type (doubling time 13–17 h), and SG mutants grew at a slower rate (doubling time > 21 h). NG mutants result from intragenic mutations, while SG mutants result from gross changes (extending beyond the *TK* gene) [20]. $KBrO_3$ predominantly induced SG mutants (Fig. 1), implying that $KBrO_3$ treatment predominantly causes gross structural changes, but not small genetic alterations such as point mutations.

3.2. Molecular analysis of TK mutants

The *TK* mutants were randomly isolated from independent cultures treated with 2.5 mM $KBrO_3$ for 4 h. Table 1 shows the cytotoxicity (RSG), mutation frequency, and proportion of SG mutants induced by $KBrO_3$. We subjected 40 induced mutants to LOH analysis. Of those, 32 (80%) were SG mutants, which corresponded closely to the percentage of SG mutants induced in the assay (74.1%), indicating that the result of LOH analysis reflected the character of the induced

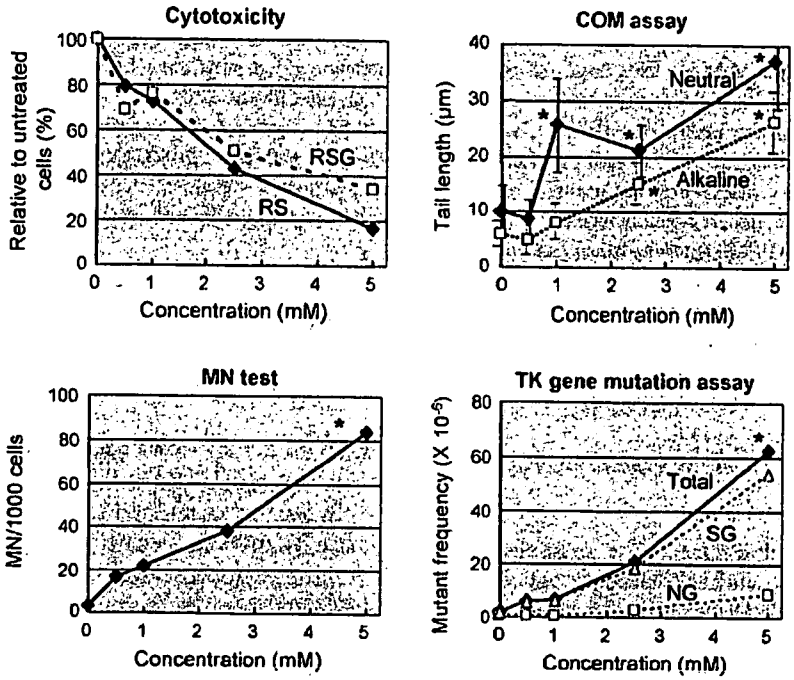

Fig. 1. Cytotoxic (relative survival, RS; relative suspension growth, RSG) and genotoxic responses (COM assay, MN test, and *TK* gene mutation assay) of TK6 cells treated with $KBrO_3$ for 4 h. Asterisk (*) statistically significant in Dunnett's test ($P < 0.05$) in COM assay, and in both pair-wise comparison and trend test ($P < 0.05$) in MN test and *TK* gene mutation assay.

mutations. Table 1 also shows the results of LOH analysis of the induced and spontaneously occurring mutants. The result of molecular analysis of spontaneous *TK* mutants was reported previously [21]. We classified the mutants into three types: non-LOH, hemizygous LOH (hemi-LOH), and homozygous LOH (homo-LOH). In general, hemi-LOH is resulted by deletion and homo-LOH is by inter-allelic homologous recombination [20]. Among the $KBrO_3$-induced mutants, 63% of NG mutants and 84% of SG mutants were hemi-LOH. In spontaneous mutants, on the other hand, majority of NG and SG mutants were non-LOH and homo-LOH, respectively. These results indicated that $KBrO_3$ predominantly induced large deletions. We previously reported the mutational spectra of *TK* mutants in TK6 cells that treated with the alkylating agent ethylmethane sulfonate (EMS), or X-irradiated [20,21]. Fig. 2 shows the comparison of the mutational spectra of spontaneous and induced *TK* mutants by EMS, X-irradiation, and $KBrO_3$. The mutation spectrum induced by $KBrO_3$ was similar to that induced by X-radiation (which also induces LOH, predominantly via deletion [21]) but not by EMS. The majority of the mutations induced by $KBrO_3$ were large deletions, but not point mutations.

Fig. 3 shows the regions of LOH and the distribution of spontaneous, X-ray-induced, and $KBrO_3$-induced

Table 1
Cytotoxic and mutational responses to $KBrO_3$, and the results of LOH analysis of normally growing (NG) and slowly growing (SG) *TK* mutants

Treatment	Cytotoxic and mutational response			LOH analysis at *TK* gene (%)			
	RSG (%)	MF ($\times 10^{-6}$)	% SG	Number	Non-LOH	Hemi-LOH	Homo-LOH
Spontaneous[a]	100	2.19	56	56			
NG mutants				19	14(74)	3(16)	2(11)
SG mutants				37	0(0)	9(24)	28(76)
$KBrO_3$ (2.5 mM)	51	29.4	74	39			
NG mutants				8	3(37)	5(63)	0(0)
SG mutants				31	1(3)	27(84)	4(13)

[a] Data from Zhan et al. [22].

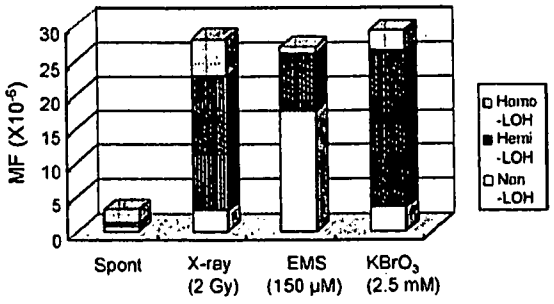

Fig. 2. *TK* mutation spectra in untreated, X-ray-treated (2 Gy), EMS-treated (150 μM, 4 h), and $KBrO_3$-treated (2.5 mM, 4 h) TK6 cells. The fraction of each mutational event was calculated by considering the ratio of NG to SG mutants and the results of molecular analysis (Table 1). The data for all but the $KBrO_3$ treatments were taken from our previous paper [20].

LOH mutants. $KBrO_3$ predominantly induced hemi-LOH, the result of large interstitial and terminal deletions, which we also frequently observed in the X-ray-induced LOH mutants. These results indicate that the genetic changes induced by $KBrO_3$ were similar to those induced by X-rays.

3.3. Gene expression analysis

Table 2 lists the genes that significantly increased expression following exposure to 2.5 mM $KBrO_3$. These genes are involved in stress response (6 genes), cell growth and DNA repair (19 genes), immune response (3 genes), apoptosis (3 genes), signal transduction (10 genes), transcription regulation (10 genes), chromosome organization (2 genes), protein modification (7 genes), energy metabolism (6 genes), lipid metabolism (2 genes), purine biosynthesis (3 genes), and unclassified functions (42 genes). Table 3 shows the genes whose expression was suppressed by the treatment. The number of up-regulated genes was greater that the number of down-regulated genes.

4. Discussion

$KBrO_3$ is a complete carcinogen, possessing both initiating and promoting activities in rodents [1]. While it shows clear positive responses in the COM assay, MN test, and chromosome aberration test using mammalian cells [4,14,17], the mutagenic potential of $KBrO_3$ in bacteria and the *Hprt* assay in Chinese hamster cells is weak or negative [1,14,17,30]. In our present study, $KBrO_3$ treatment strongly induced *TK* gene mutations. The reason we observed the induction of gene mutations and others did not is that $KBrO_3$ induces detectable mutagenecity in the *TK* gene but are only weakly mutagenic or non-mutagenic in the *Hprt* gene and in microbial assays [20]. The lower mutation frequency in the *Hprt* gene is due to the low recovery of large deletions, which are not detected because they are lethal. $KBrO_3$ is positive in mouse lymphoma cell assays that target the *Tk* gene [5]. In in vivo genotoxicity tests, $KBrO_3$ strongly induces MN in male ddY mice but is only weakly mutagenic in the *gpt* mutation assay in transgenic mice, which mainly detects point mutations and small deletions [31]. These results indicate that the property of genotoxicity

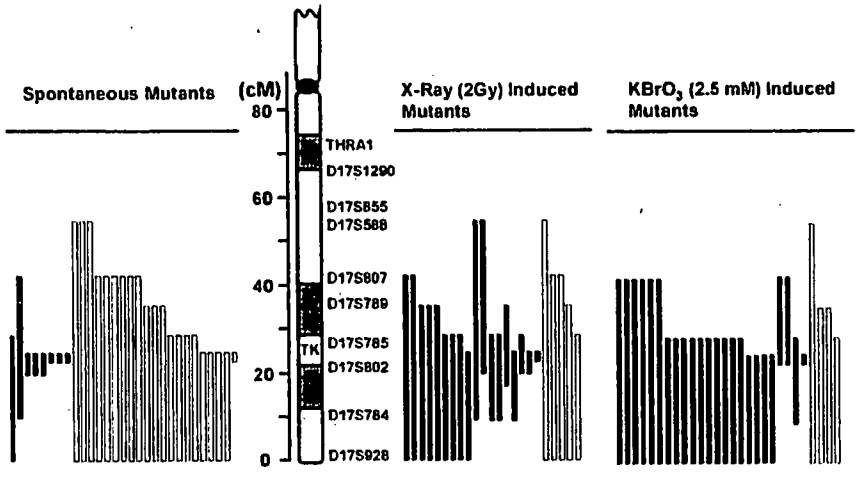

Fig. 3. The extent of LOH at the *TK* locus of TK6 cells that were untreated, X-ray-irradiated (2 Gy), or exposed to $KBrO_3$ (2.5 mM, 4 h). We examined 10 microsatellite loci on chromosome 17q that are heterozygous in TK6 cells. The human *TK* locus maps to 17q23.2. Open and closed bars represent homozygous LOH and hemizygous LOH, respectively. The length of the bar indicates the extent of the LOH. We analyzed 28 LOH mutants (4 NG and 24 SG). The data on spontaneous and X-ray-induced mutants were taken from our previous paper [20].

Table 2
Genes whose expression was up-regulated by $KBrO_3$ (2.5 mM, 4 h)

	Gene symbol	Ratio	Gene title
Stress response	CAT	2.77	Catalase
	DNAJC7	2.33	DnaJ (Hsp40) homolog, subfamily C, member 7
	FKBP5	2.87	FK506 binding protein 5
	HSPA8	3.02	Heat shock 70 kDa protein 8
	HSPCB	3.21	Heat shock 90 kDa protein 1, beta
	HSPD1	1.83	Heat shock 60 kDa protein 1
DNA repair, cell cycle, cell growth	BUB1	4.51	BUB1 budding uninhibited by benzimidazoles 1 homolog
	CCND2	5.08	Cyclin d2
	CCT2	3.33	Chaperonin containing TCP1, subunit 2 (beta)
	DKC1	2.37	Dyskeratosis congenita 1, dyskerin
	ENO1	2.10	Enolase 1 (alpha)
	HMGB1	2.16	High-mobility group box 1
	MAPRE1	2.32	Microtubule-associated protein, RP/EB family, member 1
	NME1	2.00	Non-metastatic cells 1, protein (NM23A) expressed in
	NOLC1	2.99	Nucleolar and coiled-body phosphoprotein 1
	NRAS	2.54	Neuroblastoma RAS viral (v-ras) oncogene homolog
	p21	3.22	Cyclin-dependent kinase inhibitor 1A (p21, Cip1)
	PPP2R1B	2.45	Protein phosphatase 2 (formerly 2A), regulatory subunit A (PR 65), beta isoform
	RAD21	2 34	RAD21 homolog
	RBBP4	2.00	Retinoblastoma binding protein 4
	RHOA	1.77	ras homolog gene family, member A
	SRPK1	2.75	SFRS protein kinase 1
	SSR1	2.66	Signal sequence receptor, alpha
Immune response	ARHGDIB	1.78	Rho GDP dissociation inhibitor (GDI) beta
	HLA-DRA	2.16	Major histocompatibility complex, class II, DR alpha
	IL2RG	2.43	Interleukin 2 receptor, gamma
Apoptosis	BCLAF1	6.42	BCL2-associated transcription factor 1
	FXR1	3.32	Fragile X mental retardation, autosomal homolog 1
	VDAC1	1.94	Voltage-dependent anion channel 1
Signal transduction	ANP32A	3.20	Acidic (leucine-rich) nuclear phosphoprotein 32 family, member A
	OGT	2.74	O-linked *N*-acetylglucosamine (GlcNAc) transferase
	PIP5K1A	4.25	Phosphatidylinositol-4-phosphate 5-kinase, type I, alpha
	PLEK	2.95	Pleckstrin
	PTPN11	2.61	Protein tyrosine phosphatase, non-receptor type 11
	SPTLC1	2.62	Serine palmitoyltransferase, long chain base subunit 1
	SRPR	2.52	Signal recognition particle receptor
Transcription regulation	CDC5L	4.37	CDC5 cell division cycle 5-like
	HNRPC	4.40	Heterogeneous nuclear ribonucleoprotein C (C1/C2)
	MED6	2.45	Mediator of RNA polymerase II transcription, subunit 6 homolog
	MED6	2.45	Mediator of RNA polymerase II transcription, subunit 6 homolog
	NO NO	2.68	Non-POU domain containing, octamer-binding
	POLR1C	2.67	Polymerase (RNA) I polypeptide C, 30 kDa
	PRPF4	2.51	PRP4 pre-mRNA processing factor 4 homolog
Chromosome organization	CBX5	2.68	Chromobox homolog 5 (HP1 alpha homolog, Drosophila)
Protein modification	CANX	2.56	Calnexin
	COPA	6.55	Coatomer protein complex, subunit alpha
	EIF2S3	2.40	Eukaryotic translation initiation factor 2, subunit 3 gamma
	EIF4B	2.86	Eukaryotic translation initiation factor 4B
	RANBP2	3.96	RAN binding protein 2
	SEC23IP	2.67	SEC23 interacting protein

Table 2 (*Continued*)

	Gene symbol	Ratio	Gene title
Energy pathway	AFURS1	2.83	ATPase family homolog up-regulated in senescence cells
	CYB5-M	2.54	Cytochrome *b*5 outer mitochondrial membrane precursor
	TOMM22	3.07	Translocase of outer mitochondrial membrane 22 homolog
Lipid metabolism	HMGCS1	2.58	3-Hydroxy-3-methylglutaryl-Coenzyme A synthase 1
	SCD	2.56	Stearovl-CoA desaturase
Purine biosynthesis	ENTPD1	2.36	Ectonucleoside triphosphate diphosphohydrolase 1
	GART	2.64	Phosphoribosylglycinamide formyltransferase
	PAICS	1.79	Phosphoribosylaminoimidazole carboxylase
Unclassified	BANF1	2.77	Barrier to autointegration factor 1
	BAT1	1.95	HLA-B associated transcript 1///HLA-B associated transcript 1
	C1orf16	2.37	Chromosome 1 open reading frame 16
	CALU	2.40	Calumenin
	DAZAP2	2.57	DAZ associated protein 2
	DDX18	2.34	DEAD (Asp-Glu-Ala-Asp) box polypeptide 18
	DHX9	9.37	DEAH (Asp-Glu-Ala-His) box polypeptide 9
	EXOSC2	3.03	Exosome component 2
	FLJ10534	2.07	Hypothetical protein FLJ10534
	FLJ10719	2.42	Hypothetical protein FLJ10719
	FLJ12973	2.76	Hypothetical protein FLJ12973
	GANAB	2.07	Glucosidase, alpha; neutral AB
	HEM1	2.37	Hematopoietic protein 1
	IGHM	2.76	Anti-HIV-1 gp120 V3 loop antibody DO142-10 light chain variable region
	IGKC	3.15	Anti-rabies virus immunoglobulin rearranged kappa chain V-region
	LIN7C	3.51	lin-7 homolog C (*C. elegans*)
	LOC54499	2.31	Putative membrane protein
	M6PR	3.59	Mannose-6-phosphate receptor
	MGC8902	2.27	Hypothetical protein MGC8902/
	MOBK1B	2.67	MOB1, Mps one binder kinase activator-like 1B (yeast)
	NS	2.15	Nucleostemin
	NUSAP1	3.25	Nucleolar and spindle associated protein 1
	OK/SW-cl.56	1.85	Beta 5-tubulin
	OPRS1	2.76	Opioid receptor, sigma 1
	PEG 10	2.50	Paternally expressed 10
	PEX19	2.34	Peroxisomal biogenesis factor 19
	PGK1	2.11	Phosphoglycerate kinase 1
	RPE	2.35	Ribulose-5-phosphate-3-epimerase
	SDBCAG84	3.16	Serologically defined breast cancer antigen 84
	SMU1	2.70	smu-1 suppressor of mec-8 and unc-52 homolog (*C. elegans*)
	TAGLN2	2.03	Transgelin 2
	UBC	2.65	Ubiquitin C
	XPNPEP1	2.84	X-prolyl aminopeptidase
	YWHAE	6.39	Tyrosine 3-monooxygenase/tryptophan 5-monooxygenase activation protein, epsilon polypeptide
	YWHAZ	2.50	Tyrosine 3-monooxygenase/tryptophan 5-monooxygenase activation protein, zeta polypeptide

of $KBrO_3$ predominantly causes gross structural changes rather than small genetic changes such as point mutations.

$KBrO_3$ generates high yields of 8OHdG DNA adducts, which is a marker of oxidative DNA damage widely used as a predictor of carcinogenesis [10]. 8OHdG has been reported to be highly mutagenic in some experiments. In cell-free system, 8OHdG induced mutation by misincorporating adenine instead of cytosine [12]. Artificially incorporated 8OHdG at specific codons in a shuttle vector system efficiently induced GC > TA transversions in mammalian cells and *E. coli* [8,32,33]. In mammalian gene mutation assays in vitro and in vivo, however, the relationship between the accumulation of 8OHdG and the induction of GC > TA transversion has not been clear. Takeuchi et al.

Table 3
Genes whose expression was down-regulated by $KBrO_3$ (2.5 mM, 4 h)

	Gene symbol	Ratio	Gene title
Cell cycle, cell growth	FH	0.51	Fumarate hydratase
	MYC	0.55	v-myc myelocytomatosis viral oncogene homolog
Signal transduction	DUSP2	0.37	Dual specificityphosphatase 2
	RRBP1	0.39	Ribosome binding protein 1 homolog 180 kDa
	TBL3	0 43	Transducin (beta)-like3
Transcription regulation	CITED2	0.45	Cbp/p300-interacting transactivator, with Glu/Asp-rich carboxy-terminal domain, 2
	KIAA1196	0.43	KIAA1196 protein
	TZFP	0 39	Testis zinc finger protein
Chromosome organization	H1FX	0.14	H1 histone family member X
Protein modification	CLTB	0.43	Clathrin, light polypeptide (Lcb)
Energy pathway	FDX1	0.45	Ferredoxin 1
	QPRT	0.41	Quinolinate phosphoribosyltransferase
	SLC39A4	0.43	Solute carrier family 39 (zinc transporter), member 4
Unclassified	BTBD2	0.35	BTB (POZ) domain containing 2
	LOC339229	0.44	Hypothetical protein LOC339229
	MGRN1	0.44	Mahogunin, ring finger 1
	MRP63	0.41	Mitochondrial ribosomal protein 63
	PHLDA1	0.43	Pleckstrin homology-like domain, family A, member 1
	PTPLA	0.37	Protein tyrosine phosphatase-like (proline instead of catalytic arginine), member a
	SPATA2	0.45	Spermatogenesis associated 2

examined the mutagenicity of a hydroxyl radical generator, *N,N'*-bis (2-hydroxyperoxy-2-methoxyethyl)-1,4,5,8-naphthalene-tetra-carboxylic diimide (NP-III). Although NP-III highly produced 8OHdG upon irradiation with UV in V79 cells, the frequency of *Hprt* gene mutation was not significantly induced [34]. Molecular analysis demonstrated the no association of induction of 8OHdG with GC > TA transversion in the *Hprt* mutants [35]. 8OHdG is mainly removed by Ogg1 protein in a manor of the base excision repair (BER) pathway. Arai et al. investigated the relationship between the accumulation of oxidative DNA damage and the induction of gene mutation using *Ogg1* deficient transgenic mice [36]. Although the 8OHdG level in kidneys of the *Ogg1* deficient mice increase 200 times of the control level after 4 weeks' $KBrO_3$ treatment, the mutation frequency in the transgenic *gpt* gene was induced by less than 10 times of the control level. The molecular analysis revealed that the fraction of GC > TA transversions did not specifically increased. These results suggest that 8OHdG-mediated base substitutions do not mainly contribute to the mutagenic process involved in $KBrO_3$-induced carcinogenesis. Other genotoxic events must be involved in the carcinogenic process.

Our present studies strongly support this hypothesis. We demonstrated that $KBrO_3$ treatment clearly induced DNA damage in both the alkaline and neutral COM assay (Fig. 1). The alkaline COM assay is capable of detecting any DNA damages including DSB, single strand breaks (SSB), alkali-labile sites, DNA–DNA/DNA–protein cross-linking, and SSB associated with incomplete excision repair sites, while the neutral COM assay allows the detection of DSB, considered to be "biologically relevant" lesion of radiation damage [24]. $KBrO_3$ may have radio-mimic genotoxicity that yields oxidative DNA damage as well as DSB. $KBrO_3$ also induced MN formation and *TK* gene mutation significantly in TK6 cells. In the *TK* gene mutation assay, $KBrO_3$ predominantly produced SG mutants, but not NG mutants (Fig. 1c), implying that gross structural changes such as deletion and recombination are associated with the mutations. Molecular analysis of the *TK* mutants confirmed the assumption. Most of *TK* mutants showed LOH mutations, not non-LOH mutations, which are mainly point mutations. Harrington-Brock et al. also demonstrated that bromate compounds significantly induced *Tk* mutations in mouse lymphoma L5178Y cells, and almost all were LOH mutations [5]. LOH can be caused by deletions,

mitotic recombination between homologous alleles, or whole chromosome loss [20]. Molecular analysis can distinguish between them and reveal the mechanism and the characteristics of the mutants. In this study, $KBrO_3$ predominantly induced large deletions that resulted in hemizygous LOH (Table 1). The large deletions were mainly terminal deletions in the proximal region of chromosome 17q, which were rarely observed in spontaneously arising *TK* mutants (Fig. 3). The mutational spectrum and LOH pattern induced by $KBrO_3$ were similar to those induced by X-irradiation (Figs. 2 and 3) [20,21]. DSBs induced X-rays cause large deletions [19,20]. When the DSBs are repaired by the non-homologous end-joining pathway, interstitial deletions result. The broken chromosome ends can be also stabilized by the addition of new telomere sequences. Because TK6 cells have high telomerase activity [20], the result is terminal deletions. Thus, the major genotoxicity of $KBrO_3$ may be due to DSBs, but not to 8OHdG converting GC > TA transversion.

Some 8OHdG lesions can convert DSBs through the BER pathway [37]. In the initial step of BER, Ogg1 removes 8OHdG by DNA glycosylase activity and nicks the DNA backbone because of its associated lyase activity. The resulting SSB is processed by an apurinic endonuclease, which generates a single nucleotide gap. The gap is filled in by a DNA polymerase and sealed by a DNA ligase [38]. Clustered 8OHdG lesions induced by $KBrO_3$ may not be appropriately repaired by BER and cause DSB, however, because it is possible that two closely opposed 8OHdGs convert two closely opposed SSBs by BER resulting DSB [39,40]. Yang et al. developed Ogg1 over-expressing TK6 cell (TK6-hOGG1) and examined cytotoxic and mutagenic responses to gamma-irradiation [41]. They demonstrated that TK6-hOGG1 cells are more sensitive than the parental TK6 cells to cytotoxicity and mutagenicity by gamma-irradiation, and most of the induced *TK* mutants in TK6-OGG1 exhibited SG phenotype, which were probably large deletion mutants resulted by DSBs. This result clearly indicates that BER pathway contributes to convert oxidative damages to DSBs. Some clustered 8OHdG induced by $KBrO_3$ may covert to DSBs in TK6 cells, because TK6 is Ogg1 proficient cells [37].

To clarify the genotoxic characteristics of $KBrO_3$, we investigated the gene expression profile using Affymetrix GeneChip® Expression analysis. Many genes were up- or down-regulated by exposure to 2.5 mM $KBrO_3$ (Tables 2 and 3). Akerman et al. investigated the alterations of gene expression profiles in ionizing radiation-exposed TK6 cells [42]. They reported a >50% increase in expression of ATF-3 (stress response), Cyclin G (cell cycle), FAS antigen (apoptosis), GADD45 (repair and apoptosis), PCNA (repair), Rad51 (repair), and p21 (cell cycle) and a 40% decrease in expression of c-Myc (transcription factor), interferon stimulatory gene factor-3 (cell signaling), and p55CDC (cell cycle). We also observed up-regulation of p21 and down-regulation of c-Myc. Up-regulation of p21, however, is observed in TK6 cells exposed to any DNA-damaging chemical [43]. Islaih et al. also demonstrated the relationship between the gene expression profiles and the DNA damaging agents using TK6 cells [43]. They examined six chemicals including H_2O_2 and bleomycin which induce oxidative DNA damage. Although 10 genes were commonly up-regulated between H_2O_2 and bleomycin treatments, these genes except for p21 were not observed in our experiment. Thus, we could not find the similarity of gene expression profile by the treatment with $KBrO_3$ to by the treatment with ionizing radiation as well as oxidative damage inducers. Comparing gene expression profiles across platforms, laboratories, and experiments must be difficult [44]. Although it is difficult to judge from the expression analysis of the single chemical, information on genes which altered their expression gives a clue to understand the mechanism of action. Firstly, predominance of DNA repair and cell cycle related genes in up-regulated genes supports the genotoxic action of $KBrO_3$. Up-regulation of stress genes and apoptosis related genes suggests an involvement of oxidative stress. Up-regulation of catalase may be responsible for the oxidative damage by $KBrO_3$ (Table 2). Unclassified genes for alteration may have a functional relationship with genotoxic mechanism.

In conclusion, $KBrO_3$ predominantly induced large deletions at chromosomal level in human TK6 cells. The major genotoxicity leading to carcinogenesis of $KBrO_3$ may be due to DSBs rather than to 8OHdG adducts that lead to GC > TA transversions, as is commonly believed.

Acknowledgments

The TK6 cell line used in this study was a kind gift of Dr. John B. Little of the Harvard School of Public Health, Boston, MA. This study was supported by Health, Welfare, and Labor Science Research Grants (H15-chem-002, H15-food-004) in Japan.

References

[1] Y. Kurokawa, A. Maekawa, M. Takahashi, Y. Hayashi, Toxicity and carcinogenicity of potassium bromate—a new renal carcinogen, Environ. Health Perspect. 87 (1990) 309–335.

[2] Y. Kurokawa, S. Aoki, Y. Matsushima, N. Takamura, T. Imazawa, Y. Hayashi, Dose–response studies on the carcinogenicity of potassium bromate in F344 rats after long-term oral administration, J. Natl. Cancer Inst. 77 (1986) 977–982.
[3] A.B. DeAngelo, M.H. George, S.R. Kilburn, T.M. Moore, D.C. Wolf, Carcinogenicity of potassium bromate administered in the drinking water to male B6C3F1 mice and F344/N rats, Toxicol. Pathol. 26 (1998) 587–594.
[4] M. Ishidate Jr., K. Yoshikawa, Chromosome aberration tests with Chinese hamster cells in vitro with and without metabolic activation—a comparative study on mutagens and carcinogens, Arch. Toxicol. Suppl. 4 (1980) 41–44.
[5] K. Harrington-Brock, D.D. Collard, T. Chen, Bromate induces loss of heterozygosity in the thymidine kinase gene of L5178Y/Tk(±)-3.7.2C mouse lymphoma cells, Mutat. Res. 537 (2003) 21–28.
[6] M. Hayashi, T. Sofuni, M. Ishidate Jr., High-sensitivity in micronucleus induction of a mouse strain (MS), Mutat. Res. 105 (1982) 253–256.
[7] M. Hayashi, M. Kishi, T. Sofuni, M. Ishidate Jr., Micronucleus tests in mice on 39 food additives and eight miscellaneous chemicals, Food Chem. Toxicol. 26 (1988) 487–500.
[8] H. Kamiya, K. Miura, H. Ishikawa, H. Inoue, S. Nishimura, E. Ohtsuka, c-Ha-ras containing 8-hydroxyguanine at codon 12 induces point mutations at the modified and adjacent positions, Cancer Res. 52 (1992) 3483–3485.
[9] A.G. Knudson, Antioncogenes and human cancer, Proc. Natl. Acad. Sci. U.S.A. 90 (1993) 10914–10921.
[10] H. Kasai, S. Nishimura, Y. Kurokawa, Y. Hayashi, Oral administration of the renal carcinogen, potassium bromate, specifically produces 8-hydroxydeoxyguanosine in rat target organ DNA, Carcinogenesis 8 (1987) 1959–1961.
[11] K.C. Cheng, D.S. Cahill, H. Kasai, S. Nishimura, L.A. Loeb, 8-Hydroxyguanine, an abundant form of oxidative DNA damage, causes G–T and A–C substitutions, J. Biol. Chem. 267 (1992) 166–172.
[12] S. Shibutani, M. Takeshita, A.P. Grollman, Insertion of specific bases during DNA synthesis past the oxidation-damaged base 8-oxodG, Nature 349 (1991) 431–434.
[13] K. Sai, C.A. Tyson, D.W. Thomas, J.E. Dabbs, R. Hasegawa, Y. Kurokawa, Oxidative DNA damage induced by potassium bromate in isolated rat renal proximal tubules and renal nuclei, Cancer Lett. 87 (1994) 1–7.
[14] G. Speit, S. Haupter, P. Schutz, P. Kreis, Comparative evaluation of the genotoxic properties of potassium bromate and potassium superoxide in V79 Chinese hamster cells, Mutat. Res. 439 (1999) 213–221.
[15] T. Umemura, K. Sai, A. Takagi, R. Hasegawa, Y. Kurokawa, A possible role for oxidative stress in potassium bromate (KBrO3) carcinogenesis, Carcinogenesis 16 (1995) 593–597.
[16] K. Fujie, H. Shimazu, M. Matsuda, T. Sugiyama, Acute cytogenetic effects of potassium bromate on rat bone marrow cells in vivo, Mutat. Res. 206 (1988) 455–458.
[17] M. Ishidate Jr., T. Sofuni, K. Yoshikawa, M. Hayashi, T. Nohmi, M. Sawada, A. Matsuoka, Primary mutagenicity screening of food additives currently used in Japan, Food Chem. Toxicol. 22 (1984) 623–636.
[18] H.L. Liber, W.G. Thilly, Mutation assay at the thymidine kinase locus in diploid human lymphoblasts, Mutat. Res. 94 (1982) 467–485.
[19] H.L. Liber, D.W. Yandell, J.B. Little, A comparison of mutation induction at the tk and hprt loci in human lymphoblastoid cells; quantitative differences are due to an additional class of mutations at the autosomal tk locus, Mutat. Res. 216 (1989) 9–17.
[20] M. Honma, Generation of loss of heterozygosity and its dependency on p53 status in human lymphoblastoid cells, Environ. Mol. Mutagen. 45 (2005) 162–176.
[21] M. Honma, M. Hayashi, T. Sofuni, Cytotoxic and mutagenic responses to X-rays and chemical mutagens in normal and p53-mutated human lymphoblastoid cells, Mutat. Res. 374 (1997) 89–98.
[22] L. Zhan, H. Sakamoto, M. Sakuraba, D.S. Wu, L.S. Zhang, T. Suzuki, M. Hayashi, M. Honma, Genotoxicity of microcystin-LR in human lymphoblastoid TK6 cells, Mutat. Res. 557 (2004) 1–6.
[23] N. Koyama, H. Sakamoto, M. Sakuraba, T. Koizumi, Y. Takashima, M. Hayashi, H. Matsufuji, K. Yamagata, S. Masuda, N. Kinae, M. Honma, Genotoxicity of acrylamide and glycidamide in human lymphoblastoid TK6 cells, Mutat. Res. 603 (2006) 151–158.
[24] S. Wada, H. Kurahayashi, Y. Kobayashi, T. Funayama, K. Yamamoto, M. Natsuhori, N. Ito, The relationship between cellular radiosensitivity and radiation-induced DNA damage measured by the comet assay, J. Vet. Med. Sci. 65 (2003) 471–477.
[25] M. Watanabe-Akanuma, T. Ohta, Y.F. Sasaki, A novel aspect of thiabendasole as a photomutagen in bacteria and cultured human cells, Mutat. Res. 158 (2005) 213–219.
[26] T. Matsushima, M. Hayashi, A. Matsuoka, M. Ishidate Jr., K.F. Miura, H. Shimizu, Y. Suzuki, K. Morimoto, H. Ogura, K. Mure, K. Koshi, T. Sofuni, Validation study of the in vitro micronuclei test in a Chinese hamster lung cell line (CHL/IU), Mutagenesis 14 (1999) 569–580.
[27] T. Omori, M. Honma, M. Hayashi, Y. Honda, I. Yoshimura, A new statistical method for evaluating of L5178Ytk± mammalian cell data using microwell method 517 (2002) 199–208.
[28] M. Honma, M. Momose, H. Tanabe, H. Sakamoto, Y. Yu, J.B. Little, T. Sofuni, M. Hayashi, Requirement of wild-type p53 protein for maintenance of chromosomal integrity, Mol. Carcinog. 28 (2000) 203–214.
[29] P.L. Olive, DNA damage and repair in individual cells: applications of the comet assay in radiobiology, Int. J. Radiat. Biol. 75 (1999) 395–405.
[30] D.E. Levin, M. Hollstein, M.F. Christman, E.A. Schwiers, B.N. Ames, A new Salmonella tester strain (TA102) with A X T base pairs at the site of mutation detects oxidative mutagens, Proc. Natl. Acad. Sci. U.S.A. 79 (1982) 7445–7449.
[31] T. Arai, V.P. Kelly, O. Minowa, T. Noda, S. Nishimura, High accumulation of oxidative DNA damage, 8-hydroxyguanine, in Mmh/Ogg1 deficient mice by chronic oxidative stress, Carcinogenesis 23 (2002) 2005–2010.
[32] F. Le Page, A. Margot, A.P. Grollman, A. Sarasin, A. Gentil, Mutagenicity of a unique 8-oxoguanine in a human Ha-ras sequence in mammalian cells, Carcinogenesis 16 (1995) 2779–2784.
[33] M.L. Wood, M. Dizdaroglu, E. Gajewski, J.M. Essigmann, Mechanistic studies of ionizing radiation and oxidative mutagenesis: genetic effects of a single 8-hydroxyguanine (7-hydro-8-oxoguanine) residue inserted at a unique site in a viral genome, Biochemistry 29 (1990) 7024–7032.
[34] T. Takeuchi, S. Matsugo, K. Morimoto, Mutagenicity of oxidative DNA damage in Chinese hamster V79 cells, Carcinogenesis 18 (1997) 2051–2055.
[35] M. Nakajima, T. Takeuchi, K. Ogino, K. Morimoto, Lack of direct involvement of 8-hydroxy-2′-deoxyguanosine in

hypoxanthine-guanine phosphoribosyltransferase mutagenesis in V79 cells treated with *N,N'*-bis(2-hydroxyperoxy-2-methoxyethyl)-1,4,5,8-naphthalenetetracarboxyli c-diimide (NP-III) or riboflavin, Jpn. J. Cancer Res. 93 (2002) 247–252.

[36] T. Arai, V.P. Kelly, K. Komoro, O. Minowa, T. Noda, S. Nishimura, Cell proliferation in liver of Mmh/Ogg1-deficient mice enhances mutation frequency because of the presence of 8-hydroxyguanine in DNA, Cancer Res. 63 (2003) 4287–4292.

[37] N. Yang, M.A. Chaudhry, S.S. Wallace, Base excision repair by hNTH1 and hOGG1: a two edged sword in the processing of DNA damage in gamma-irradiated human cells, DNA Repair (Amst.) 5 (2006) 43–51.

[38] G. Slupphaug, B. Kavli, H.E. Krokan, The interacting pathways for prevention and repair of oxidative DNA damage, Mutat. Res. 531 (2003) 231–251.

[39] K. Tian, M. McTigue, S.C. de los, Sorting the consequences of ionizing radiation: processing of 8-oxoguanine/abasic site lesions, DNA Repair (Amst.) 1 (2002) 1039–1049.

[40] M.E. Lomax, S. Cunniffe, P. O'Neill, Efficiency of repair of an abasic site within DNA clustered damage sites by mammalian cell nuclear extracts, Biochemistry 43 (2004) 11017–11026.

[41] N. Yang, H. Galick, S.S. Wallace, Attempted base excision repair of ionizing radiation damage in human lymphoblastoid cells produces lethal and mutagenic double strand breaks, DNA Repair (Amst.) 3 (2004) 1323–1334.

[42] G.S. Akerman, B.A. Rosenzweig, O.E. Domon, C.A. Tsai, M.E. Bishop, L.J. McGarrity, J.T. Macgregor, F.D. Sistare, J.J. Chen, S.M. Morris, Alterations in gene expression profiles and the DNA-damage response in ionizing radiation-exposed TK6 cells, Environ. Mol. Mutagen. 45 (2005) 188–205.

[43] M. Islaih, B.W. Halstead, I.A. Kadura, B. Li, J.L. Reid-Hubbard, L. Flick, J.L. Altizer, D.J. Thom, D.K. Monteith, R.K. Newton, D.E. Watson, Relationships between genomic, cell cycle, and mutagenic responses of TK6 cells exposed to DNA damaging chemicals, Mutat. Res. 578 (2005) 100–116.

[44] C.L. Yauk, M.L. Berndt, A. Williams, G.R. Douglas, Comprehensive comparison of six microarray technologies, Nucleic Acids Res. 32 (2004) e124.

Neuroscience 147 (2007) 153–163

RETINOIC ACIDS ACTING THROUGH RETINOID RECEPTORS PROTECT HIPPOCAMPAL NEURONS FROM OXYGEN-GLUCOSE DEPRIVATION-MEDIATED CELL DEATH BY INHIBITION OF C-JUN-N-TERMINAL KINASE AND p38 MITOGEN-ACTIVATED PROTEIN KINASE

Y. SHINOZAKI,[a] Y. SATO,[b]* S. KOIZUMI,[a] Y. OHNO,[c] T. NAGAO[c] AND K. INOUE[d]

[a]*Division of Pharmacology, National Institute of Health Sciences, 1-18-1 Kamiyoga, Setagaya, Tokyo 158-8501, Japan*

[b]*Division of Cellular and Gene Therapy Products, National Institute of Health Sciences, 1-18-1 Kamiyoga, Setagaya, Tokyo 158-8501, Japan*

[c]*National Institute of Health Sciences, 1-18-1 Kamiyoga, Setagaya, Tokyo 158-8501, Japan*

[d]*Department of Molecular and System Pharmacology, Graduate School of Pharmaceutical Sciences, Kyushu University, Maidashi3-1-1, Higashi-ku, Fukuoka 812-8582, Japan*

Abstract—Retinoic acids (RAs), including all-*trans* retinoic acid (ATRA) and 9-*cis* retinoic acid (9-*cis* RA), play fundamental roles in a variety of physiological events in vertebrates, through their specific nuclear receptors: retinoic acid receptor (RAR) and retinoid X receptor (RXR). Despite the physiological importance of RA, their functional significance under pathological conditions is not well understood. We examined the effect of ATRA on oxygen/glucose-deprivation/reperfusion (OGD/Rep)-induced neuronal damage in cultured rat hippocampal slices, and found that ATRA significantly reduced neuronal death. The cytoprotective effect of ATRA was observed not only in cornu ammonis (CA) 1 but also in CA2 and dentate gyrus (DG), and was attenuated by selective antagonists for RAR or RXR. By contrast, in the CA3 region, no protective effects of ATRA were observed. The OGD/Rep also increased phosphorylated forms of c-jun-N-terminal kinase (P-JNK) and p38 (P-p38) in hippocampus, and specific inhibitors for these kinases protected neurons. ATRA prevented the increases in P-JNK and P-p38 after OGD/Rep, as well as the decrease in NeuN and its shrinkage, all of which were inhibited by antagonists for RAR or RXR. These findings suggest that the ATRA signaling via retinoid receptors results in the inhibition of JNK and p38 activation, leading to the protection of neurons against OGD/Rep-induced damage in the rat hippocampus.

*Corresponding author. Tel: +81-3-3700-1141x275; fax: +81-3-3707-6950.
E-mail address: yoji@nihs.go.jp (Y. Sato).

Abbreviations: ATRA, all-*trans* retinoic acid; CA, cornu ammonis; DG, dentate gyrus; ERK, extracellular signal-regulated kinase; Hanks' BSS, Hanks' balanced salt solution; JNK, c-jun-N-terminal kinase; MAPK, mitogen-activated protein kinase; MKP-1, mitogen-activated protein kinase phosphatase-1; OGD, oxygen and glucose deprivation; PBS-T, phosphate-buffered saline with 0.3% Triton X-100, pH 7.6; P-ERK, phosphorylated extracellular signal-regulated kinase; PI, propidium iodide; P-JNK, phosphorylated c-jun-N-terminal kinase; P-p38, phosphorylated p38; RA, retinoic acid; RAR, retinoic acid receptor; Rep, reperfusion; RXR, retinoid X receptor; ssDNA, single-stranded DNA; TBS/T, Tris-buffered saline containing 0.1% Tween-20; 9-*cis* RA, 9-*cis* retinoic acid.

Key words: retinoic acid, RAR, RXR, MAPK, ischemia.

Retinoids, including vitamin A (retinol) and its derivatives, regulate a wide range of biological processes, such as cell growth and differentiation, development, and carcinogenesis (Chambon, 1996; Maden, 2001). Retinoic acids (RAs) regulate the expression of a large number of genes upon binding and activation of the nuclear retinoid receptors, retinoic acid receptors (RARα, RARβ, and RARγ) and retinoid X receptors (RXRα, RXRβ, and RXRγ) (Chambon, 1996; Maden, 2001). RARs are activated by all-*trans* retinoic acid (ATRA) and 9-*cis* retinoic acid (9-*cis* RA), whereas RXRs are activated by 9-*cis* RA (Chambon, 1996) and other non-retinoid lipid ligands such as docosahexaenoic acid (de Urquiza et al., 2000). In the presence of RA, these receptors act as transcription factors in forms of RAR/RXR heterodimers or RXR homodimers, which bind to retinoic acid response elements (RARE) in the promoter of target genes (Chambon, 1994; Kastner et al., 1997). RA has multiple effects on physiological functions in the adult brain, such as long-term potentiation and long-term depression (Chiang et al., 1998; Misner et al., 2001) and neurogenesis (Haskell and LaMantia, 2005; Jacobs et al., 2006). RA also plays significant roles under pathological conditions. For example, in mesangial cells and fibroblast, ATRA has a protective effect against H_2O_2 via receptor-mediated mechanisms (Konta et al., 2001; Xu et al., 2002). Although several lines of evidence link RA to some psychiatric pathogenesis (Strahan and Raimer, 2006), defects in retinoid signaling have been associated with neurodegenerative disorders such as Alzheimer's disease and amyotrophic lateral sclerosis (Corcoran et al., 2002; Goodman and Pardee, 2003). However, the role of RA signaling in other pathological conditions such as ischemia in the brain remains unclear.

The mitogen-activated protein kinase (MAPK) family, which plays an essential role in the transduction of environmental stimuli to the nucleus, consists of three commonly recognized subgroups: extracellular signal-regulated kinase (ERK), c-jun-N-terminal kinase (JNK), also known as the stress activated protein kinase (SAPK) and p38 kinase. JNK and p38 kinase are activated in response to cellular stresses like ischemia in the heart, kidney and brain (Hu and Wieloch, 1994; Mizukami et al., 1997; Yin et al., 1997; Herdegen et al., 1998; Walton et al., 1998) and have been associated with neuronal cell death (Xia et al., 1995; Watson et al., 1998; Namgung and Xia, 2000). JNK

0306-4522/07$30.00+0.00
doi:10.1016/j.neuroscience.2007.04.032

and p38 kinase activate downstream molecules such as caspase-3 (Kuan et al., 2003; Lee and Lo, 2003), Bax (Okuno et al., 2004), MAPK-activated protein kinase 2 (MAPKAP2) (Wang et al., 2002) and activator protein-1 (AP-1) (Ishikawa et al., 1997; Yokoo and Kitamura, 1997; Behrens et al., 1999) thereby leading of neuronal cell death. In contrast, ERK1/2 is mainly activated by various neurotransmitters, hormones and growth factors, controlling transcription factor activity to induce various physiological responses, such as cell proliferation or differentiation (Boulton et al., 1991; Marshall, 1995; Segal and Greenberg, 1996). However, ERK1/2 is also activated by various types of stress such as oxidative or shear stress, controlling the survival of cells (Xia et al., 1995; Guyton et al., 1996; Wang et al., 1998). Recent studies have shown that ATRA protects neurons from amyloidβ (Sahin et al., 2005) and staurosporine (Ahlemeyer and Krieglstein, 1998). Based on the findings above, we hypothesized that RA signaling would be inversely associated with neuronal cell death under pathological conditions. To test our hypothesis, we examined the effect of ATRA on hippocampal neurons against oxygen and glucose deprivation/reperfusion (OGD/Rep)-induced neuronal damage, and found that ATRA protected hippocampal neurons against cell death. We also found that the neuroprotective effect of ATRA was mediated by inhibition of OGD/Rep-induced activation of JNK and p38 kinase.

EXPERIMENTAL PROCEDURES

Materials

Propidium iodide (PI) and anti-β-actin antibody were purchased from Sigma Chemical Co. (St. Louis, MO, USA). The sources of the following chemicals are shown in parentheses: ATRA and 9-*cis* RA (Wako Pure Chemicals, Osaka, Japan), U0126, SB203580, SP600125 and anti-NeuN antibody (Calbiochem Biosciences, Inc., San Diego, CA, USA). LE135 (Li et al., 1999) and HX531 (Ebisawa et al., 1999) were synthesized and graciously provided by Dr. Koichi Shudo (Research Foundation Itsuu Laboratory, Tokyo, Japan). Antibodies against phosphorylated extracellular signal-regulated kinase 1/2 (P-ERK1/2), phosphorylated p38 (P-p38), phosphorylated c-jun-N-terminal kinase (P-JNK), and active caspase-3 were purchased from Cell Signaling Technology (Beverly, MA, USA). The sources of the following antibodies are shown in parentheses: single-stranded DNA (ssDNA) antibody (DAKO Cytomation, Glostrup, Denmark), RAR and RXR antibodies (Santa Cruz Biotechnology, Inc., Santa Cruz, CA, USA).

Organotypic hippocampal slice culture

Organotypic slice cultures of the hippocampus were prepared using the culture method described by Skrede and Westgaard (1971) All animals were treated in accordance with the laboratory animal care guidance of the National Institute of Health Sciences at Tokyo and the guidelines of the International Council for Laboratory Animal Science (ICLAS; http://www.iclas.org/). Every effort was made to minimize the number of experimental animals used and their suffering. Eleven-day-old Wistar rats were decapitated, and the brains were rapidly dissected and placed in a Petri dish containing ice-cold 1× Hanks' balanced salt solution (Hanks' BSS, from Gibco, Rockville, MD, USA). Both right and left hippocampi were isolated and sectioned into 300 μm transverse slices with a McIlwain tissue chopper (Mickle Laboratory Engineering Co. Ltd., Goose Green, UK). The slices were then carefully separated and transferred onto porous membrane inserts of six-well culture plates (two or three slices per insert) (Millicell-CM, Millipore, Billerica, MA, USA). To reach the level of insert membrane, 800 μL culture medium was added to the lower compartment of each well, and the culture plates were then placed in a 37 °C humidified incubator enriched with 5% CO_2. The cell culture medium consisted of 50% Minimum Essential Medium with 25 mM Hepes, 25% Hanks' BSS and 25% heat-inactivated horse serum, which were supplemented with 2 mM L-glutamine, 100 U/mL penicillin and 100 μg/mL streptomycin. On the next day, the culture medium was replaced with fresh medium and from then on changed once every 2 days. Hippocampal slices were used for each experiment after incubation for 12 days.

OGD

Hippocampal slices were exposed to OGD using an anaerobic chamber. The slices were transferred in dishes with 800 μl glucose-free DMEM containing (mg/L): 200 $CaCl_2$, 400 KCl, 97.67 $MgSO_4$, 6400 NaCl, 3700 $NaHCO_3$, 125 NaH_2PO_4 and then placed into an airtight chamber containing 95% N_2, 5% CO_2 (37 °C) for 40 min. After OGD, the slices were placed back in the incubator in normal culture medium and incubated for 24 h. RAs were added to the culture medium 24 h before OGD and during Rep. Antagonists for RAR and RXR were added to the medium 30 min before and during the RA treatment. Inhibitors of MAPKs were added to the slices simultaneously at Rep.

Immunohistochemistry

The hippocampal slices were fixed with 4% paraformaldehyde for 1–2 h and rinsed two times (each 10 min at room temperature) with PBS-T (phosphate-buffered saline with 0.3% Triton X-100, pH 7.6). After blocking with 3% normal goat serum in PBS-T for 2 h at room temperature, the slices were incubated with the primary antibody (1/1000-fold dilution in PBS-T with 3% goat serum) for 48 h at 4 °C, followed by incubation with the Alexa Fluor-conjugated secondary antibody (1/1000-fold dilution, Molecular Probes, Eugene, OR, USA) for 3 h at room temperature. Images were collected with a MRC-1024 laser-scanning microscope (Bio-Rad, Richmond, CA, USA) using ×4 or ×20 objective lenses. For comparisons of double-stained patterns, images were processed using Photoshop CS (Adobe Systems, Mountain View, CA, USA). High magnification images of the NeuN/active caspase-3/ssDNA/P-p38/P-JNK staining are shown for the cornu ammonis 1 (CA1) region, unless otherwise indicated.

Western blotting analysis of slices

Slices were homogenized in 100 μl lysis buffer (10 mM Tris, pH 7.5, 150 mM NaCl, 1 mM EDTA, 1 mM EGTA, 1% Triton X-100, 0.1% SDS, 1 mM sodium orthovanadate, 1% deoxycholate, and 10 μg/mL each aprotinin, bestatin, pepstatin A, leupeptin), using Tissue Lyser (Qiagen, Hilden, Germany). The proteins were separated in 10% SDS-PAGE gels and transferred to PVDF membranes. The membranes were blocked for 1 h in Tris-buffered saline containing 0.1% Tween-20 (TBS/T) and 5% non-fat dry milk at room temperature. Then the membranes were incubated with the primary antibody (1/1000-fold dilution in TBS/T containing 5% BSA) overnight at 4 °C. After three washes with TBS/T, the membranes were incubated with a horseradish peroxidase–conjugated anti-rabbit antibody (1/2000 dilution in TBS/T containing 5% non-fat dry milk) for 1 h at room temperature. The membranes were washed with TBS/T three times, and the proteins were visualized by chemiluminescence.

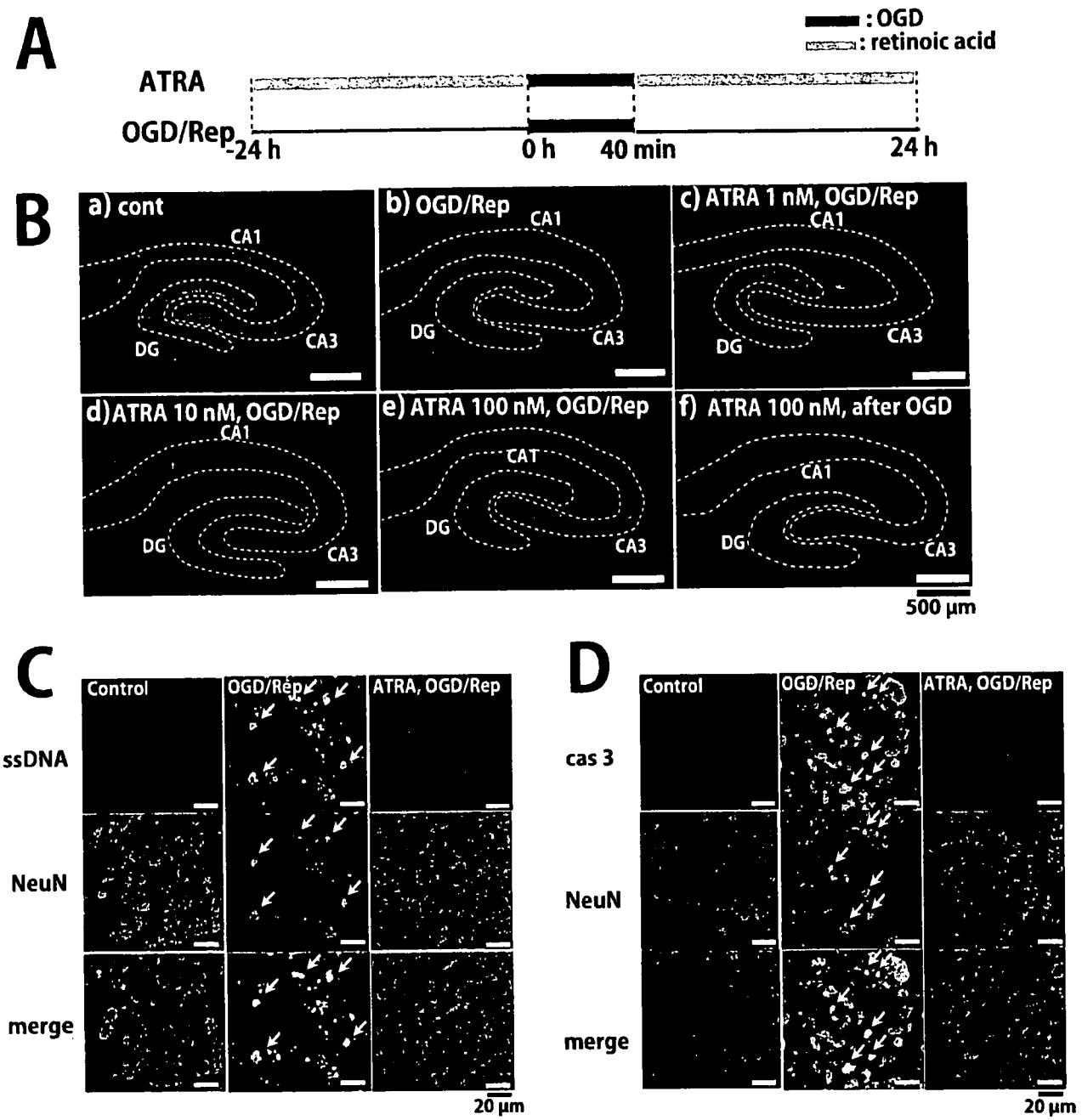

Fig. 1. The protective effect of ATRA on OGD/Rep-induced damage of neurons in the organotypic hippocampal slice culture. (A) A schematic diagram of the experimental protocol. Hippocampal slices were treated with ATRA 24 h before OGD and during Rep. The slices were subjected to OGD for 40 min followed by 24 h Rep. (B) The protective effect of ATRA on neurons in hippocampal slices. (a) NeuN staining of control slices. Incubation period for 12 days did not affect the NeuN staining of hippocampal slices. (b) OGD/Rep-induced neuronal loss. OGD/Rep dramatically decreased NeuN staining in hippocampal slices. (c–e) Effect of ATRA on the OGD/Rep-induced decrease of NeuN staining in hippocampal slices. At 1 nM, ATRA did not have a significant effect on NeuN staining decreased by OGD/Rep (c). At ≥10 nM ATRA prevented the decrease in NeuN by OGD/Rep (d, 10 nM; e, 100 nM). (f) The protective effect of ATRA after OGD. ATRA (100 nM) after OGD also had protective effects. Scale bar=500 μm. (C) DNA damage associated with the OGD/Rep-induced decrease in NeuN. In control, ssDNA signals were hardly detected (left, upper panel). OGD/Rep increased ssDNA signals (center, upper panel), which were shrunken and merged with NeuN signals (center, lower panel, arrows). ATRA prevented the changes in NeuN signals (right, middle panel) and reversed the increased ssDNA signals (right, upper panel). (D) OGD/Rep activates caspase-3 in neuronal cells. In control, the signals for active caspase-3 were barely detected (left, upper panel). OGD/Rep induced an increase in active caspase-3 (center, upper panel), which was colocalized with NeuN signals (center, arrows). ATRA prevented the OGD/Rep-induced changes in NeuN and active caspase-3 (right, middle and upper panels). Scale bar=20 μm.

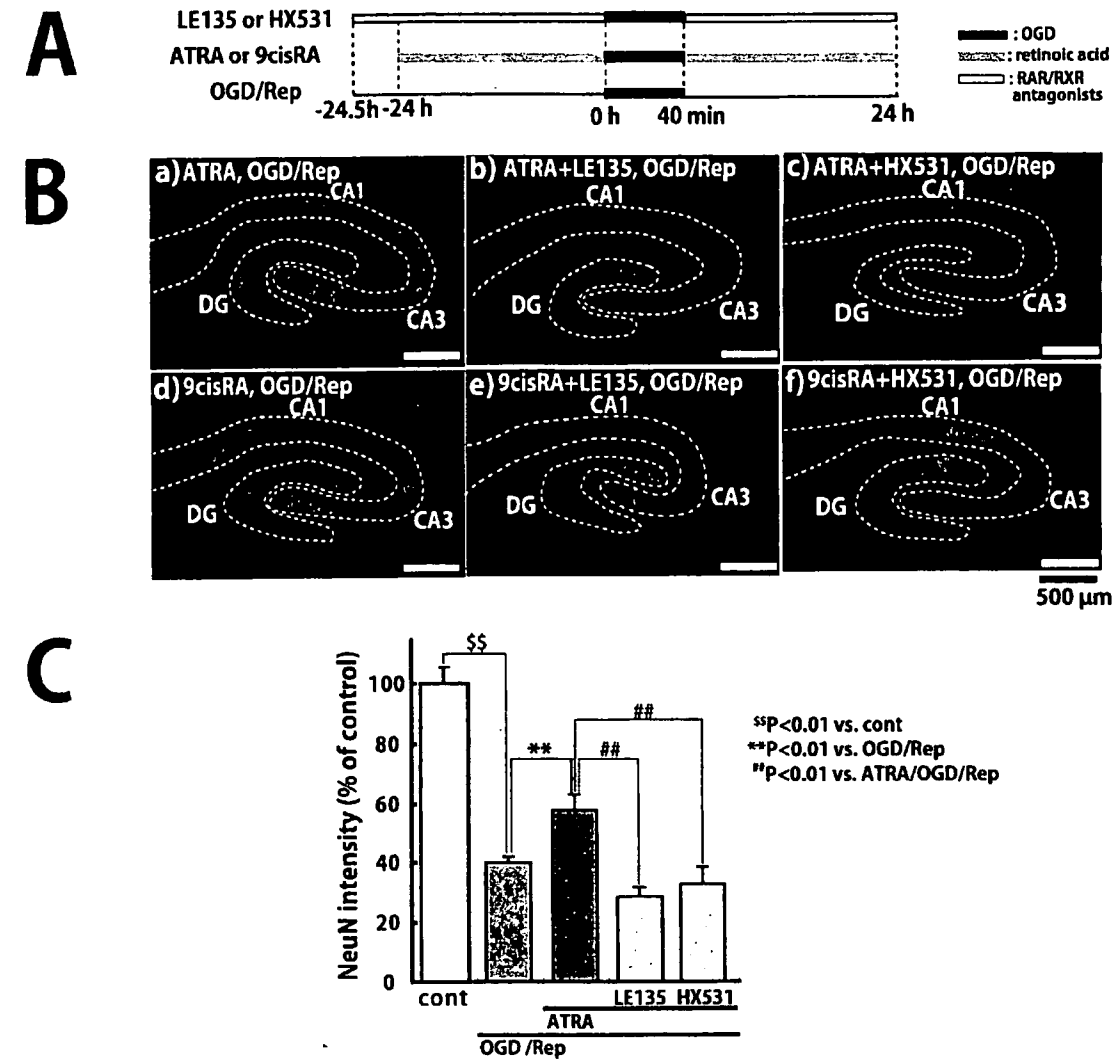

Fig. 2. The inhibitory effect of RAR/RXR antagonists on the RA-induced protective effect. (A) A schematic diagram of the experimental protocol. Hippocampal slices were treated with RAs (ATRA or 9-*cis* RA) 24 h before OGD and during Rep. Antagonists for RAR and RXR were added to the culture medium 30 min before and during RA treatment. The slices were subjected to OGD for 40 min and Rep for 24 h. (B) RAR/RXR antagonists inhibit the neuroprotective effect of RA. The effect of ATRA (a) was inhibited by both RAR antagonist LE135 (1 μM) (b) and RXR antagonist HX531